title

Direct and biodiversity-mediated effects of climate on grassland productivity across the Alps

Running title : Abiotic vs. biotic control on productivity

Authors :

Gaüzère Pierre[1], Maria Hällfors[2], Jussi Mäkinen[2], Philippe Choler[1], Risto K. Heikkinen[2], Romain Goury[1], Joaquim Estopinan[1], Cyrille Violle[3], Franziska Schrodt[4], Sara Si Moussi[1], Mickaël Hedde[5], Luca Santini[6], Wilfried Thuiller[1]

Affiliations :

[1] Univ. Grenoble Alpes, Univ. Savoie Mont Blanc, CNRS, LECA, F-38000 Grenoble, France

[2] Finnish Environment Institute, Helsinki, Finland

[3] CEFE, Univ Montpellier, CNRS, EPHE, IRD, INRAE, Montpellier, France

[4] School of Geography, University of Nottingham, Nottingham, UK

[5] Eco&Sols, INRAE, IRD, CIRAD, Institut Agro, University Montpellier, Montpellier, France

[6] Department of Biology and Biotechnologies “Charles Darwin”, Sapienza University of Rome, Rome, Italy

Keywords: ecosystem productivity, climate variability, alpine grasslands, functional traits, biodiversity–ecosystem functioning, remote sensing, causal inference, environmental heterogeneity

Abstract

Understanding how climate shapes ecosystem productivity through both energetic constraints and biodiversity-mediated pathways remains a major challenge in global change ecology, particularly in mountain grasslands where rapid warming and strong environmental gradients interact. Here, we disentangle and map direct climatic controls on productivity from indirect effects mediated by canopy functional structure across the European Alps. Using Sentinel-2 time series (2017–2024), we quantified canopy functional structure from spectral proxies of pigment investment and water status, functional richness, and vegetation productivity using near-infrared reflectance of vegetation (NIRv). We combined causal inference with piecewise structural equation modelling to partition total climate effects into direct and trait-mediated components and used varying-coefficient models to evaluate how these pathways vary along environmental gradients.

We identified two concurrent pathways linking climate to productivity. Warmer growing seasons directly increased productivity but simultaneously reduced canopy pigment investment and water status, generating negative indirect effects that partly offset direct gains. Greater winter snow accumulation reduced productivity both directly, by shortening the effective growing season, and indirectly, through increases in canopy water content associated with lower productivity. Climatic water deficit produced opposing effects, with weakly positive direct impacts counteracted by negative indirect effects mediated by pigment-related traits, resulting in minimal net productivity change. Trait diversity showed relatively weak climate responses and modest contributions to indirect effects.

Environmental context strongly modulated climate–vegetation relationships. Baseline temperature and moisture availability most strongly shaped climate effects on canopy traits and productivity, whereas biodiversity–functioning relationships varied little across space. Strongest positive productivity responses to warming occurred in moist, mid-elevation regions, while responses weakened or became neutral at high elevations, snow-rich areas, and dry sites.

Together, our findings show that short-term productivity responses in mountain grasslands arise from the balance between direct energetic constraints and biodiversity-mediated physiological adjustments, and that this balance shifts predictably along macroclimatic gradients.

Main text

Introduction

Understanding how ecosystem functioning emerges from the interplay between abiotic constraints and biotic organization is a central challenge in ecology (Chapin et al., 2000). Climate sets fundamental limits on biological activity by controlling energy, water availability, and seasonality. Yet, ecosystems often respond to climatic variation in ways that cannot be explained solely by direct climatic effects (Saugier, 2001). Instead, biodiversity - through the composition, structure, and diversity of species and their functional traits - can modulate, buffer, or amplify climate effects on ecosystem functioning (Chapin et al., 2000; Lavorel & Garnier, 2002). However, the relative importance of direct climatic controls versus biodiversity-mediated pathways remains a major unresolved question, particularly concerning how this varies across large spatial extents. Mountain grasslands offer a compelling context to address this challenge. Along steep environmental gradients, productivity may shift from energy-limited to water-limited regimes (Denissen et al., 2022), while plant communities simultaneously reorganise in terms of dominant strategies and functional diversity. In such systems, climate change may influence productivity directly, for example through temperature-driven changes in growing-season length or snow dynamics (Körner, 2021a; Piao et al., 2011; Wipf & Rixen, 2010), and indirectly through shifts in trait composition and functional diversity that alter community-level resource use (Lavorel & Garnier, 2002; Suding et al., 2008).

Biodiversity and ecosystem responses to climate change can be constrained by local environmental conditions, so that similar climatic anomalies produce contrasting ecological outcomes depending on the baseline abiotic context (Mod et al., 2016; Suding et al., 2008). Biodiversity–functioning relationships likely depend on local differences in abiotic constraints, resource availability, and community composition (Leibold et al., 2017). Mapping such spatial heterogeneity can reveal under which conditions biodiversity and ecosystem functioning are most sensitive to climate change, and where trait composition and diversity most strongly impact ecosystem functioning. In addition, revealing this heterogeneity helps identify where conservation or management interventions may be most effective. Yet, despite decades of research on biodiversity–ecosystem functioning, we still lack spatially explicit, causal quantification of how much ecosystem productivity is controlled directly by climate versus indirectly through biodiversity, and how this balance varies across environmental contexts in natural systems.

Within the biodiversity–ecosystem functioning framework, several non-exclusive mechanisms have been proposed. Ecosystem functioning may be driven primarily by the traits of dominant species (mass-ratio effects), enhanced by functional complementarity among species, or stabilized by insurance effects arising from asynchronous responses to environmental variability (Grime, 1998; Loreau & Hector, 2001). Trait Driver Theory (TDT) formalizes this view by predicting that ecosystem functioning is governed by the distribution of trait values expressed within communities, with directional selection toward phenotypes maximizing resource use efficiency under given environmental constraints (Enquist et al., 2015). While these mechanisms are experimentally well-supported, their relative importance in shaping productivity across natural landscapes remains debated. Translating these mechanisms from experimental settings to heterogeneous natural landscapes requires observations that capture how functional strategies are expressed across space and time.

Recent advances in optical remote sensing allow vegetation functional properties to be monitored continuously across large spatial extents (Cavender-Bares, Schneider, et al., 2022; Ustin & Gamon, 2010). Leaf pigments, water content, and canopy structure leave consistent spectral signatures that reflect plant physiological strategies and responses to stress (Cavender-Bares, Gamon, et al., 2022; Gamon et al., 2019;

Ustin & Gamon, 2010). Spectral indices derived from multispectral imagery therefore provide integrative proxies of realized canopy functional structure and physiological state, capturing both functional dominance and within-species physiological adjustment. When combining climatic time series with such proxies of vegetation functional state and ecosystem productivity, it is possible to investigate climate–biodiversity–ecosystem functioning relationships beyond experimental plots and across large extents and heterogeneous landscapes. However, the volume and dimensionality of remote-sensing time series also pose a challenge: patterns derived from thousands of plots and multiple correlated indices are potentially confounded by shared physiological processes. Causal inference approaches are therefore essential to explicitly detect and separate direct climatic effects from biodiversity-mediated pathways, and identify when observed associations reflect genuine mediation rather than shared environmental forcing (Van Cleemput et al., 2024).

Here, we operationalize biodiversity as the realized community functional structure expressed in the canopy, quantified through the composition and diversity of spectral traits related to pigments and water status. These traits reflect the distribution of physiological strategies actually expressed by the species community. Hence, biodiversity can act either as a buffer that stabilizes productivity under stress or as an amplifier that enhances climatic responses depending on the local functional composition or resource context. However, disentangling their roles requires separating direct climatic effects (e.g. through energy or water limitation) from indirect biodiversity-mediated effects, which remain difficult to distinguish across spatial and temporal gradients in natural systems (Dee et al., 2023; van der Plas, 2019).

To address these challenges and explicitly link the theoretical expectations above to spatially explicit data, we combine metrics derived from remote-sensing time series with causal modeling approaches (Ferraro et al. 2019; Dee et al. 2023). This allows us to formally identify and quantify mediating pathways by linking climate variability, biodiversity dynamics, and ecosystem productivity. We measure climate variability through interannual anomalies in temperature, water, and snow; biodiversity dynamics through canopy functional structure such as spectral proxies of canopy pigment investment and water status, and their functional richness, which can vary through shifts in species relative abundances and identities as well as within-species physiological adjustment; and ecosystem productivity by integrating NIRv across the growing season (Cavender-Bares, Schneider, et al., 2022; Ustin et al., 2009). We test four inter-linked hypotheses (Fig. 1).

- (H1) Interannual climatic anomalies modify canopy functional structure - reflected in spectral trait composition and diversity - through stress filtering and physiological adjustment.
- (H2) Variation in canopy functional structure mediates ecosystem productivity, with pigment- and water-related traits exerting stronger control than trait diversity - consistent with mass-ratio and trait-driver expectations.
- (H3) Climate additionally affects productivity directly through energy and water limitation, with warmer growing seasons expected to enhance productivity, greater snow accumulation and higher water deficit to reduce it.
- (H4) The strength and direction of all pathways are mediated by background environmental conditions, such as average climate, soil conditions, and topography.

Directional and mechanistic expectations associated with each hypothesis are detailed in Supporting Information S1. To test these predictions across natural grasslands of the Alps, we quantified how annual climatic anomalies translated into anomalies of canopy functional structure and productivity. We then partitioned total climate effects on productivity into 1) direct and 2) indirect trait-mediated components using piecewise Structural Equation Models (SEMs). Finally, we mapped how these pathways vary along

background gradients in climate, soil, and topography. Such an analytical framework enables spatially explicit attribution of climate–biodiversity–ecosystem functioning pathways.

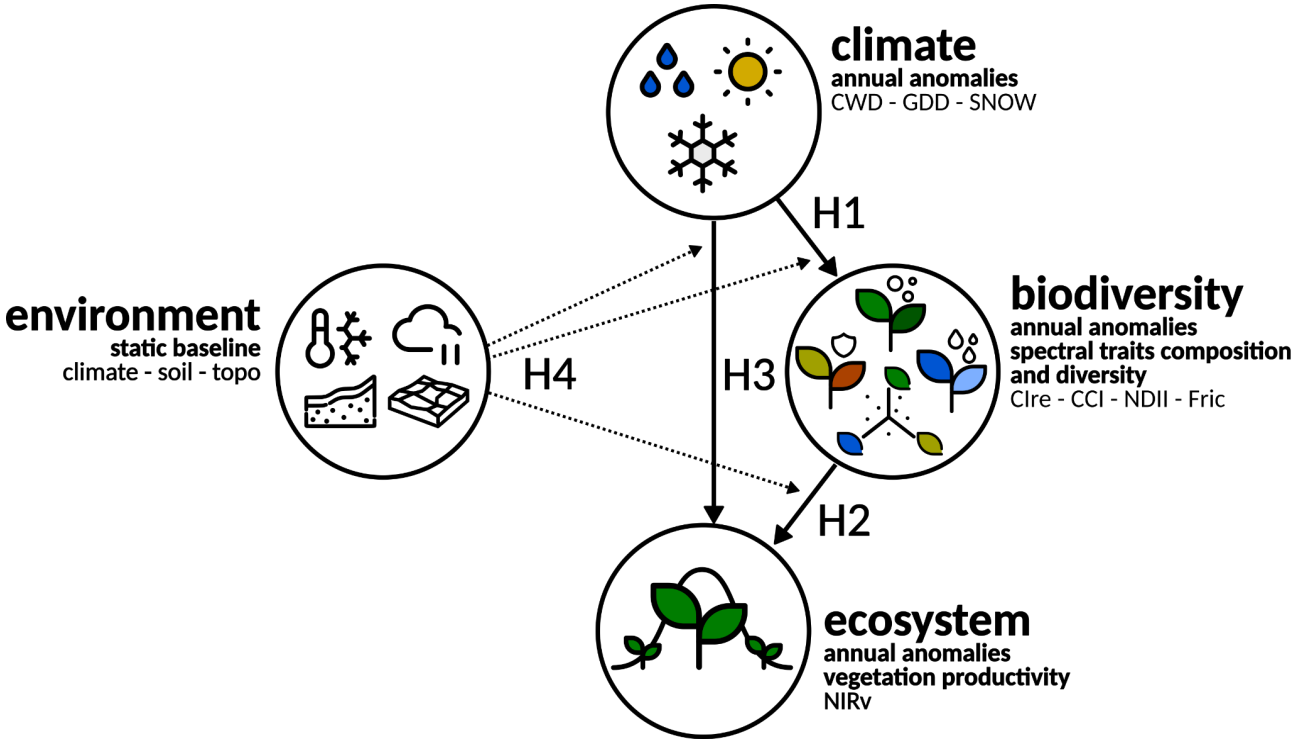

Figure 1. Causal pathways linking climate change drivers, biodiversity dynamics, and ecosystem productivity, including study hypotheses (H). H1) Annual climatic anomalies influence biodiversity through changes in composition and diversity, quantified here as spectral trait composition (CIre, CCI, NDII) and spectral trait diversity (FRic). CIre is a red-edge chlorophyll index reflecting canopy chlorophyll content and potential photosynthetic capacity; CCI is a carotenoid–chlorophyll index sensitive to shifts in photoprotective pigment investment; NDII is a near-infrared water index related to canopy water status; and FRic is the volume of spectral trait space occupied by the community, reflecting functional richness. H2) These biodiversity changes, in turn, affect ecosystem productivity dynamics, measured as near-infrared reflectance of vegetation (NIRv), a proxy for vegetation productivity. H3) Climate change also directly influences ecosystem productivity through energy and water limitation. H4) Each of these causal pathways can be modulated by baseline environmental conditions, such as average climate, prevailing soil and topography, which vary across space. Solid arrows indicate causal effect pathways, while dashed arrows indicate moderation of these effects by background environmental conditions. All hypotheses are tested using causal modeling with detailed mechanistic predictions provided in Supporting Information Text S1.

Methods

Study area and sampling design

We focused on natural grasslands located above 1,000 m a.s.l. across the European Alps, a system characterized by strong climatic gradients, short growing seasons, and relatively homogeneous low-intensity land use. Mountain grasslands are predominantly managed through traditional summer grazing, with limited fertilization or irrigation, allowing vegetation dynamics to be interpreted primarily in relation to climatic variability rather than abrupt land-use change. Using land-cover and elevation data, we delineated a continuous grassland mask across the Alpine arc and randomly selected 10,000 plot centroids within this area. Each plot was defined as a circular buffer with a 60 m radius - a spatial scale chosen to integrate multiple Sentinel-2 pixels while being small enough to capture relatively homogeneous grassland

conditions. All analyses were conducted at the plot level. Detailed geospatial processing steps are provided in the Supporting Information Text S3.

Figure 2. Study area and sampling design. Natural grasslands (identified based on CORINE Land Cover 2018, class 3.2.1) located above 1,000 m across the Alpine arc visualized over a shaded-relief background. Black points mark randomly selected plot centroids, around which 60-m-radius circular plots were defined (buffers not displayed to enhance visibility).

We defined our study area as natural grasslands located above 1000 m asl within the European Alps and delineated it in Google Earth Engine. First, we loaded CORINE Land Cover 2018 (100 m) data and retained pixels classified as “Natural grasslands” (class 3.2.1). We used elevation obtained from the Copernicus GLO30 Digital Elevation Model (DEM) thresholded at >1000 m. To isolate the Alps, we intersected these pixels with a hand-drawn polygon approximating the Alpine arc. The “grassland” and “elevation” masks were combined and clipped to this polygon to define the study area. To avoid border effects (i.e., ecotones and minor boundary errors), we further eroded the borders of the resulting mask by removing a 100 m inward buffer, thereby excluding edge pixels and ensuring that the subsequent 60 m plot buffers remained fully within the grassland patches. To sample analysis points, we drew a random sample of 10,000 points within this study area and defined each point as the center of a geodesic circular polygon with a 60-m radius, hereafter referred to as “plot”.

Remotely sensed vegetation functioning and biodiversity proxies

We characterized interannual variation in vegetation functioning and canopy properties using satellite observations from 2017–2024. All vegetation metrics were derived from Sentinel-2 surface reflectance imagery and processed consistently across years. Analyses were restricted to the growing season (April–October), and standard quality masks were applied to remove clouds, snow, and ice. To ensure reliable estimation of vegetation properties in heterogeneous alpine terrain, analyses were restricted to pixels with high fractional vegetation cover, thereby excluding rocky, sparsely vegetated, or mixed surfaces

known to bias pigment- and water-related indices. Plot-level values were obtained by aggregating all retained pixels within each plot.

Canopy functional structure as biodiversity. We used three spectral indices to characterize canopy functional structure: a red-edge chlorophyll index (CIre), a carotenoid–chlorophyll index (CCI), and a near-infrared water index (NDII). These indices capture complementary aspects of plant physiological functioning, including photosynthetic pigment investment, photoprotective demand, and canopy water status. Instead of interpreting these indices as direct measurements of taxonomic or trait composition, we treat them as proxies of realised canopy functional structure, integrating the functional properties expressed by the plant community in a given year. Variation in these indices can arise from shifts in species dominance (mass-ratio effects) and/or within-species physiological and phenotypic adjustment to interannual climatic variability. Consequently, the biodiversity-mediated effects estimated in our analyses should be interpreted as operating through changes in expressed canopy functional structure rather than through taxonomic turnover alone. To quantify functional diversity, we computed functional richness (FRic) based on the multivariate distribution of spectral traits within each plot and year, capturing the range of physiological strategies expressed at the canopy level.

Ecosystem productivity. Ecosystem productivity was quantified using near-infrared reflectance of vegetation (NIRv), a satellite-based proxy of gross primary productivity that integrates canopy structure, light absorption, and photosynthetic activity. NIRv was aggregated across the growing season to capture cumulative productivity at the plot level.

Because climate influences integrated canopy properties that jointly affect multiple spectral bands, spectral traits and NIRv are expected to covary to some extent. In our causal framework, this shared variance is interpreted as an ecologically meaningful signal rather than redundant radiometric information. Importantly, spectral traits summarize near-peak canopy physiological state, whereas productivity integrates vegetation functioning over the full growing season, ensuring that mediators and outcomes capture related but distinct aspects of ecosystem functioning. We therefore did not orthogonalize spectral traits against NIRv, as doing so would remove the specific biophysical signal through which climate is hypothesized to affect productivity via canopy functional structure.

Climate variability and environmental context.

We characterized interannual climatic variability using three variables representing the primary abiotic constraints on mountain grassland functioning: thermal energy availability, water limitation, and snow dynamics. Thermal conditions were quantified using growing degree days above 5 °C (GDD), water limitation using growing-season climatic water deficit (CWD), and snow dynamics using maximum winter snow water equivalent (SWE). These variables were selected based on well-established theoretical and empirical links between climate, plant physiological activity, and growing-season length in mountain ecosystems. Climate time series were extracted for each plot for the period 2017–2024 from gridded reanalysis and climatological datasets. Although the native spatial resolution of these products is coarser than the plot resolution, our inference targets within-plot interannual anomalies rather than fine-scale spatial gradients rendering this approach suitable. Climate variables should therefore be interpreted as year-to-year deviations experienced in each plot relative to its mean climatic context, rather than as precise microclimatic estimates.

To characterize the background environmental context, we compiled a set of static environmental variables describing long-term climatic conditions, soil properties, and topography across a continuous 100x100m

grid covering the study area (Fig. 2). These variables primarily vary across space and are assumed to remain constant over the study period. They were used as effect modifiers to test whether the strength and direction of climate–biodiversity–productivity relationships vary along environmental gradients, rather than as direct drivers of vegetation dynamics.

Study design and causal inference framework

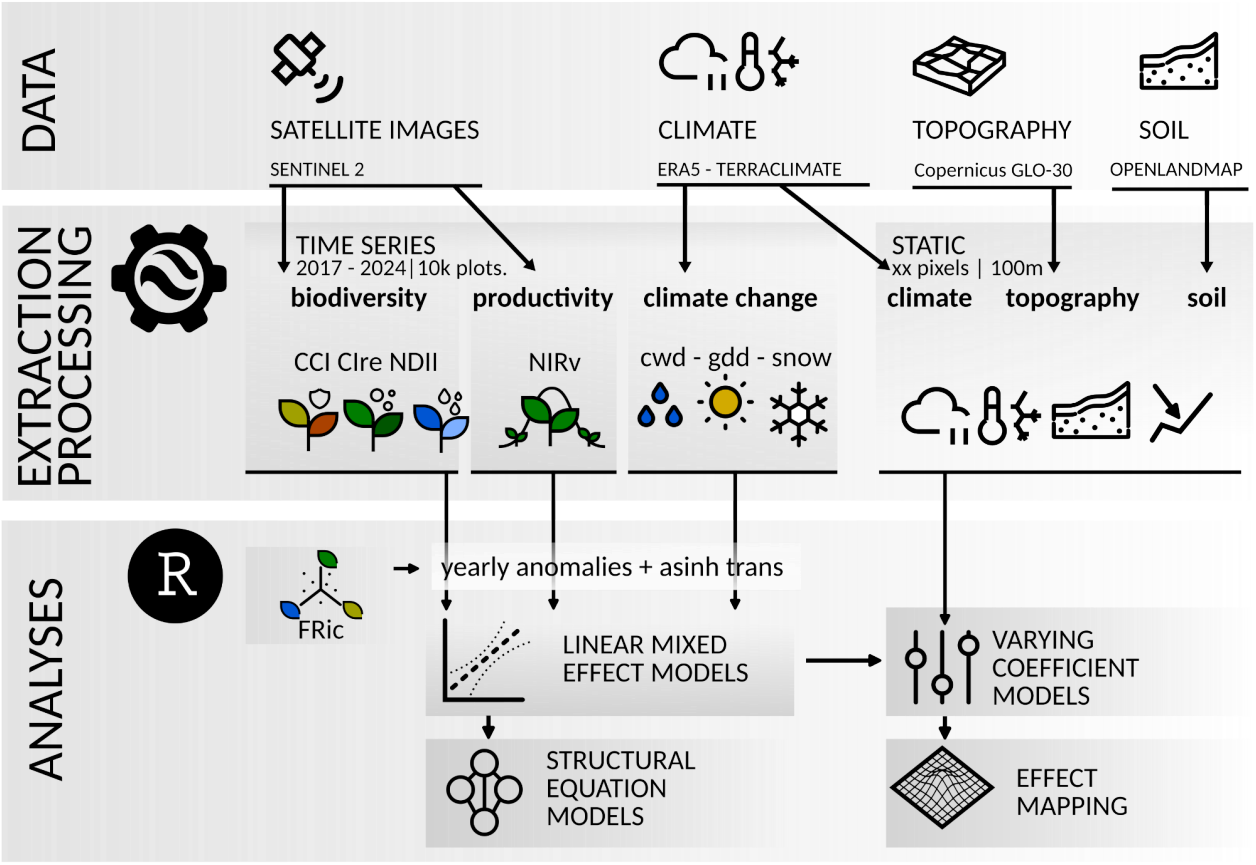

Figure 3. Analysis workflow. From satellite (Sentinel-2) and climate reanalyses (era5/terraclimate), we derived annual time series (2017–2024 ~10,000 plots) of spectral-trait composition (CCI, CIre, NDII), spectral-trait diversity (e.g. FRic), and productivity (NIRv), together with interannual climate anomalies (GDD, cwd, swe) and static environment grids (climate, topography from copernicus glo-30, and soils from openlandmap). Time-varying variables were converted to **within-plot yearly anomalies** and transformed with inverse hyperbolic functions (**asinh**). Inference used **linear mixed-effects models** with plot and year effects to estimate within-plot responses. **Piecewise structural equation models** combined these fits to separate direct climate effects on productivity from indirect effects via biodiversity. Spatial heterogeneity was assessed with **varying-coefficient LMMs**, where climate slopes vary by baseline environment. The fitted effects were projected over the alpine raster stack to produce effect and uncertainty maps.

Estimating causal effects. Our analyses targeted how year-to-year climatic anomalies influence canopy functional structure and, in turn, ecosystem productivity. We addressed three linked questions: (i) how climate affects canopy functional structure and diversity (H1), (ii) how canopy functional structure influences productivity (H2), and (iii) how climate affects productivity directly and indirectly through biodiversity-mediated pathways (H3). To isolate within-plot effects, all time-varying variables were expressed as interannual anomalies by subtracting plot-specific means. This design removed all time-invariant differences among plots, such as persistent soil conditions or long-term management, and focuses inference on temporal climatic forcing. Models included plot-level random effects to account for repeated measurements and year fixed effects to absorb shocks common to all plots in a given year. We used linear mixed models to estimate within-plot relationships among climate, canopy functional structure,

and productivity. Outcomes and predictors were analysed on an inverse hyperbolic sine scale, which stabilizes variance and accommodates zero and negative anomaly values. As a robustness check, core models were re-estimated using two-way fixed-effects regressions, yielding consistent results (Text S4).

Partitioning direct and biodiversity-mediated climate effects. To separate direct climatic effects on productivity from indirect effects operating through canopy functional structure, we linked the fitted mixed models into a piecewise structural equation framework. Climate–biodiversity models quantify how climatic anomalies modify canopy functional structure and diversity, while productivity models including both climate and biodiversity quantify how these changes translate into variation in NIRv. For each climatic driver, the total effect on productivity was decomposed into a direct component and indirect components mediated by canopy functional structure and diversity. Statistical uncertainty in direct, indirect, and total effects was quantified by propagating uncertainty from the fitted models.

Spatial heterogeneity in climate effects. To assess how climate impacts vary across environmental contexts, we fitted varying-coefficient mixed models allowing within-plot climate effects to depend linearly on static environmental variables describing average climate, soils, and topography. These models quantify how background environmental conditions modulate climate–biodiversity and climate–productivity relationships. Using these models, we mapped spatial variation in local climate effects across the Alpine grasslands, restricting predictions to environmental conditions represented in the data. Uncertainty in mapped effects was quantified by propagating parameter uncertainty from the fitted models. Additional methodological details, including data sources, preprocessing steps, statistical formulations, robustness checks, and uncertainty propagation, are provided in (Text S3).

Results

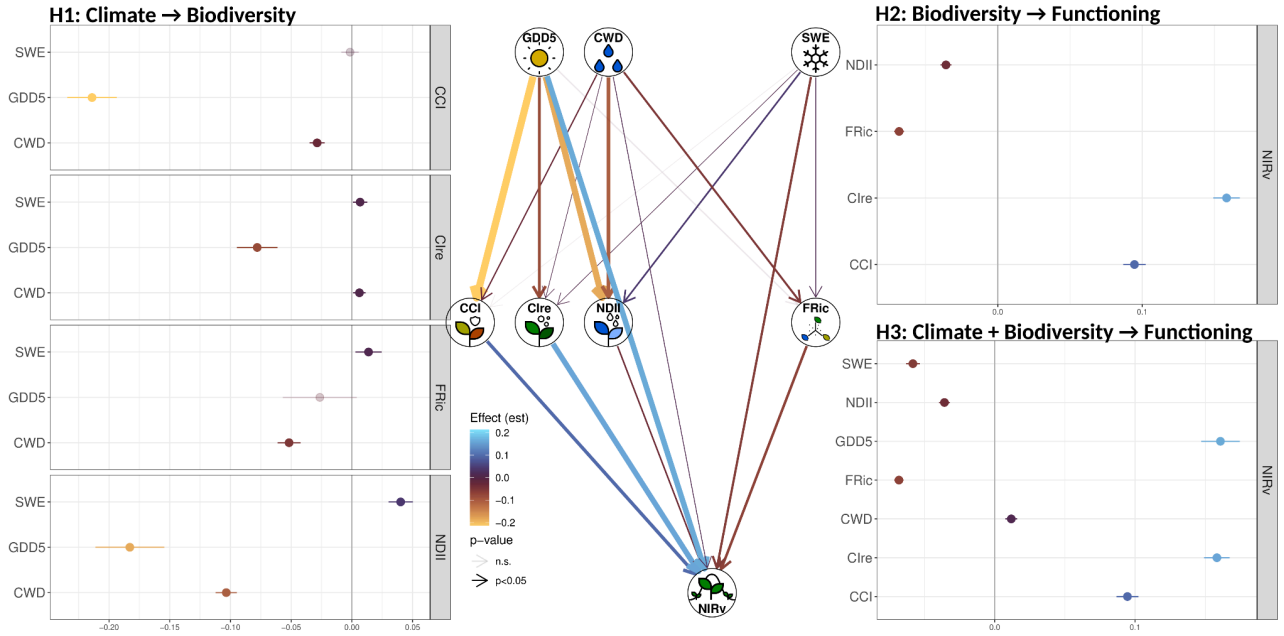

Figure 4. Within-plot (demeaned) LMM effects and the corresponding piecewise SEM. Left: H1 climate → biodiversity; top-right: H2 biodiversity → productivity (NIRv); bottom-right: H3 climate + biodiversity → NIRv. Points are *asinh*-scale estimates with 95% CIs, transparent points are non-significant effects (p-value > 0.05). In the center: graph of the SEM with, with coefficient effect size is depicted through the color palette and its absolute value by the thickness of the arrow lines.

Direct and biodiversity-mediated effects of climate anomalies on grassland productivity

Across the Alps, interannual climate variability affected productivity through two concurrent pathways: a direct energy-driven pathway and an indirect pathway mediated by canopy functional structure. Temperature accumulation generally increased productivity directly but reduced pigment-related traits, whereas snow accumulation consistently reduced productivity through both pathways.

H1: Interannual climate anomalies were associated with systematic variation in canopy spectral traits (Fig. 4, left panel). Photoprotective pigment investment (CCI) showed an average decline with higher growing-season thermal accumulation (GDD) and higher climatic water deficit (CWD), but no clear association with winter snow water equivalent (SWE). Chlorophyll-related spectral composition (CIre) was lower in years with higher GDD, and showed a weak positive association with CWD and SWE. Canopy water status (NDII) declined with both higher GDD and higher CWD, and increased with higher SWE. Spectral functional richness (FRic) showed weaker responses to climate than trait composition. FRic decreased with higher CWD and weakly increased with higher SWE, but did not respond to GDD.

H2: Vegetation productivity, quantified using growing-season NIRv, varied with canopy spectral traits (Fig. 4, top right panel). NIRv increased with higher values of CIre and CCI, and decreased with higher NDII and FRic.

H3: When accounting for biodiversity-mediated pathways, interannual climate anomalies exerted direct effects on productivity (Fig. 4, bottom right panel). NIRv increased with higher GDD and decreased with higher SWE, while the direct effect of CWD on NIRv was weak and slightly positive. Among biodiversity variables included in the model, CIre and CCI retained positive associations with NIRv, whereas NDII and FRic were negatively associated.

Putting the pathways together: structural equation model. The structural equation model identified two concurrent pathways linking interannual climate variability to ecosystem productivity (Fig. 5): an indirect pathway mediated by canopy spectral traits and a direct pathway from climate anomalies to productivity. The relative magnitudes of direct, indirect, and total effects are summarized in Figure S5.

For growing-season thermal accumulation (GDD), the indirect pathway operated primarily through changes in pigment-related traits. Higher GDD was associated with lower CIre, and because CIre had a positive effect on NIRv, this indirect pathway contributed negatively to productivity. In contrast, the direct effect of GDD on NIRv was positive and of larger magnitude than the summed indirect effects, resulting in a net positive total effect of GDD on productivity. Decomposition of indirect effects showed that this negative mediation was dominated by pigment-related traits, with negligible contribution from functional richness (Fig. S6). For snow water equivalent (SWE), both pathways contributed in the same direction. Higher SWE increased NDII, which was weakly negatively associated with NIRv, yielding a negative indirect effect. In addition, SWE exerted a negative direct effect on NIRv. Together, these pathways resulted in a clearly negative total effect of SWE on productivity (Fig. S5). For climatic water deficit (CWD), indirect and direct pathways opposed each other. Indirect effects via pigment-related traits contributed negatively to productivity, whereas indirect effects via NDII and the direct effect of CWD on NIRv were weakly positive (Fig.S6). These opposing contributions largely cancelled each other out, leading to a small net positive total effect of CWD on productivity.

Environmental modulation and spatial variation of effects

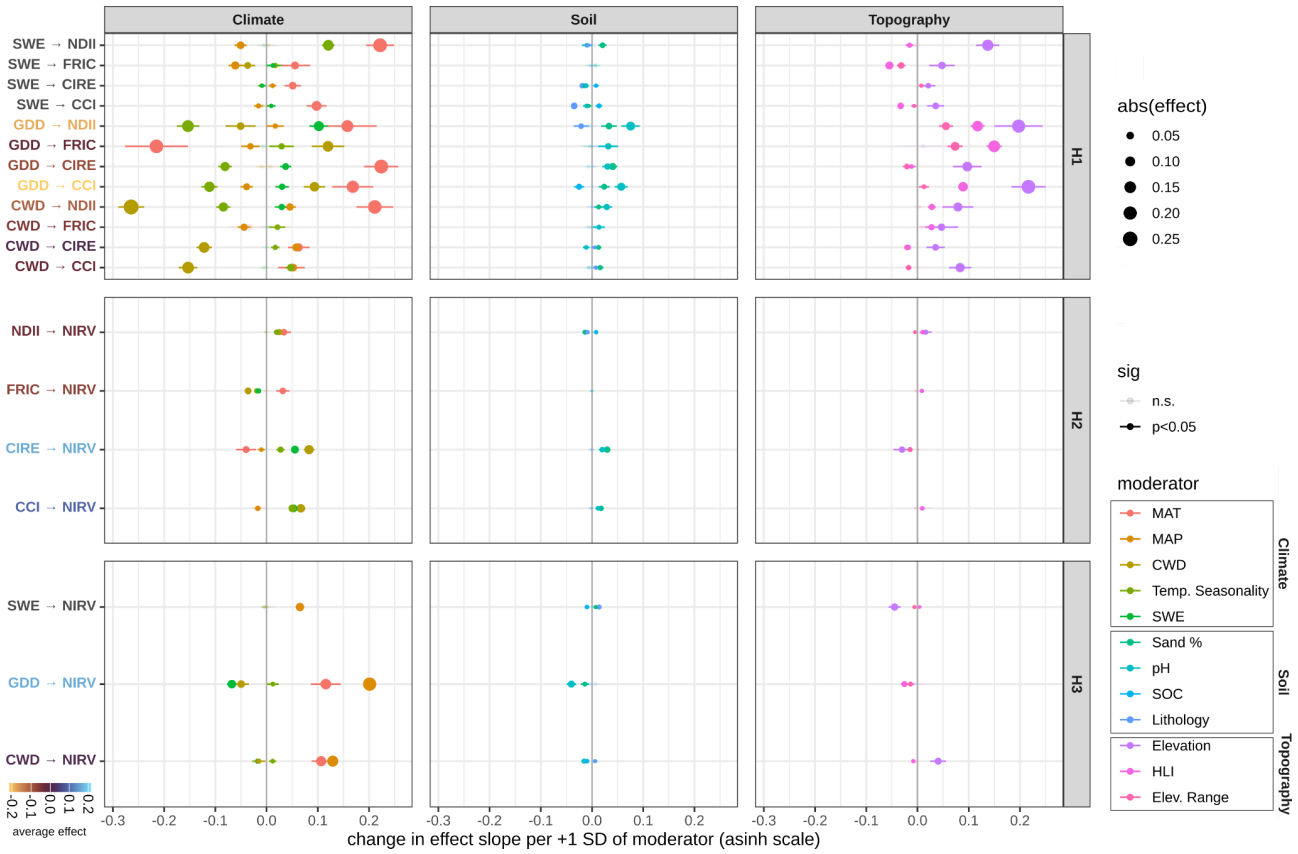

Figure 5. Environmental modulation of causal effects on pathways (varying-coefficient LMM). Panels show how the baseline environment modified the within-plot effects in the causal models. Rows correspond to pathways: H1 (climate → biodiversity), H2 (biodiversity → NIRv), and H3 (direct climate → NIRv, conditional on traits). Within-plot effects are on the y axis, with text color showing the average effect (as in Fig. 4, color scale "average effect"). Columns group baseline moderators into Climate, Soil, and Topography. Points show environmental moderator coefficients (change in the focal effect per +1 SD of the moderator) and line ranges the +1 SD of the moderator (at the *asinh* scale), with point size corresponding to magnitude and point color to moderator identity. The color of the y-axis labels indicate which moderator was the main driver of the causal effect. Negative estimates indicate that the focal effect became more positive or less negative as the moderator increased, while positive estimates indicate that it became more negative or less positive.

H4: Environmental context significantly modulated several climate–biodiversity and climate–productivity relationships (Fig. 5). Across pathways, baseline climatic variables accounted for a larger share of effect heterogeneity than soil or topographic variables.

In climate ⟶ biodiversity pathways (H1, Fig. 5, top panels), the effects of climate anomalies on canopy functional structure depended on average climate, local soil, and topography conditions. Mean annual temperature (MAT) and long-term climatic water deficit (CWD) emerged as the strongest moderators. In particular, the negative effect of GDD on CCI reduced and reversed under warmer and drier baseline conditions. Similarly, the negative effect of interannual CWD on NDII was stronger in locations characterized by higher long-term water deficit. Soil properties had weaker overall moderating effects , although pH was significantly associated with variation in selected trait responses. Topographic variables, including mean elevation and heat load index (HLI), also significantly modulated several H1 pathways, with higher elevation mitigating the negative effects of GDD on NDII and CCI. In biodiversity ⟶ productivity pathways (H2, Fig. 5, middle panels), environmental modulation was generally weak. Effect sizes linking spectral traits and functional richness to NIRv showed limited variation across baseline climatic, soil, and topographic gradients. In the climate ⟶ productivity pathways (H3; Fig. 5, bottom panels), baseline climatic conditions again emerged as the dominant moderators. Mean annual precipitation (MAP) and mean annual

temperature (MAT) were significantly associated with spatial variation in climatic effects on productivity. In particular, the positive effect of GDD on NIRv increased with higher long-term moisture availability.

Focus on GDD→CCI environmental modulation. Baseline environmental conditions explained 19.7% of the plot-to-plot variation in the effect of growing-season thermal accumulation (GDD) on canopy photoprotective pigment investment (CCI). Although the average GDD → CCI effect was negative (Fig. 4), its magnitude varied strongly across environmental gradients (Fig. 5). Long-term aridity and mean elevation were the strongest moderators, both attenuating the negative GDD → CCI effect and leading to neutral or weakly positive effects in the most arid locations and at higher elevations. Soil pH had a weaker but significant moderating influence, whereas higher temperature seasonality strengthened the negative GDD → CCI effect. Spatial projections revealed a marked geographic structure (Fig. 6), with strongly negative effects in the northern and eastern part of the Alps and weaker or near-zero effects in much of the south-western part of the Alps, becoming locally positive in the southernmost areas. Topographic modulation generated finer-scale variation, with more negative effects in valley bottoms, weaker effects at higher elevations, and weaker responses on south-facing compared to north-facing slopes.

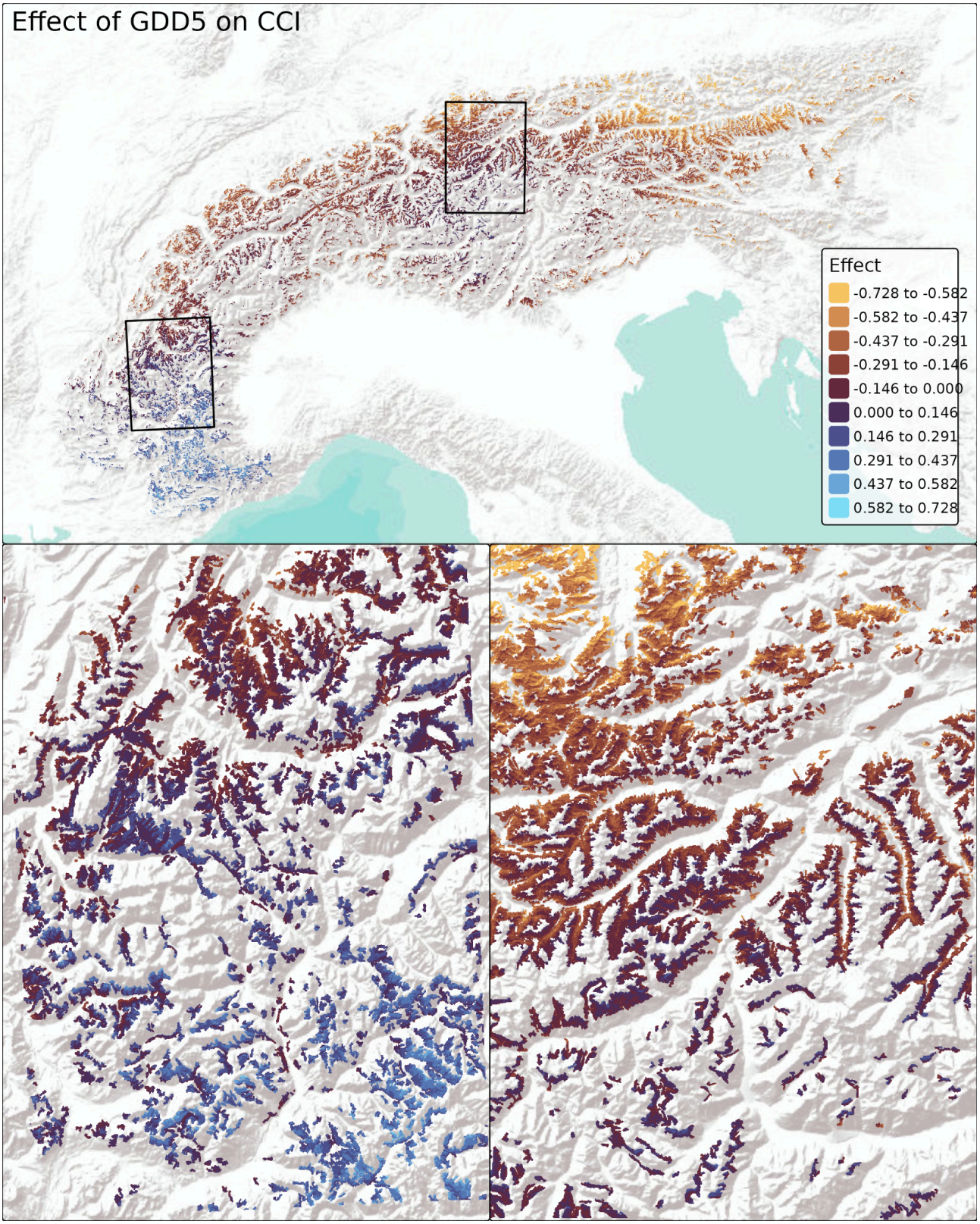

Figure 6. Predicted spatial distribution of the within-plot GDD→CCI effect from the varying-coefficient LMM. Colors show the magnitude and direction of the GDD→CCI effect on the *asinh* scale (blue = more negative; orange = more positive).

Focus on GDD→NIRv environmental modulation. The direct effect of growing-season thermal accumulation on productivity (GDD → NIRv) showed substantial spatial heterogeneity, with static environmental variables explaining approximately 30% of plot-to-plot variation in effect size. Mean annual precipitation (MAP) was the strongest positive moderator (Fig. 5), with moister sites exhibiting stronger positive productivity responses to warmer growing seasons. In contrast, mean elevation and snow water

equivalent (SWE) were the strongest negative moderators, substantially reducing the magnitude of the GDD → NIRv effect. Additional variables, including long-term aridity (CWD), soil pH, soil sand content, and heat load index (HLI), further weakened the positive GDD → NIRv relationship. Spatial projections (Fig. 7) showed strong positive responses concentrated in relatively moist, mid-elevation regions, whereas weak or neutral responses dominated high-elevation areas, snow-rich plateaus, and dry, high-insolation sectors of the south-western Alps. Fine-scale variation was also evident, with weaker responses in valley floors than on adjacent higher terrain and slightly stronger responses on south-facing slopes.

Additional interpretations of the environmental modulation of particular effects, such as GDD→NDII, CIre→NDII,FRic→NIRv, are available in Figure S7**.**

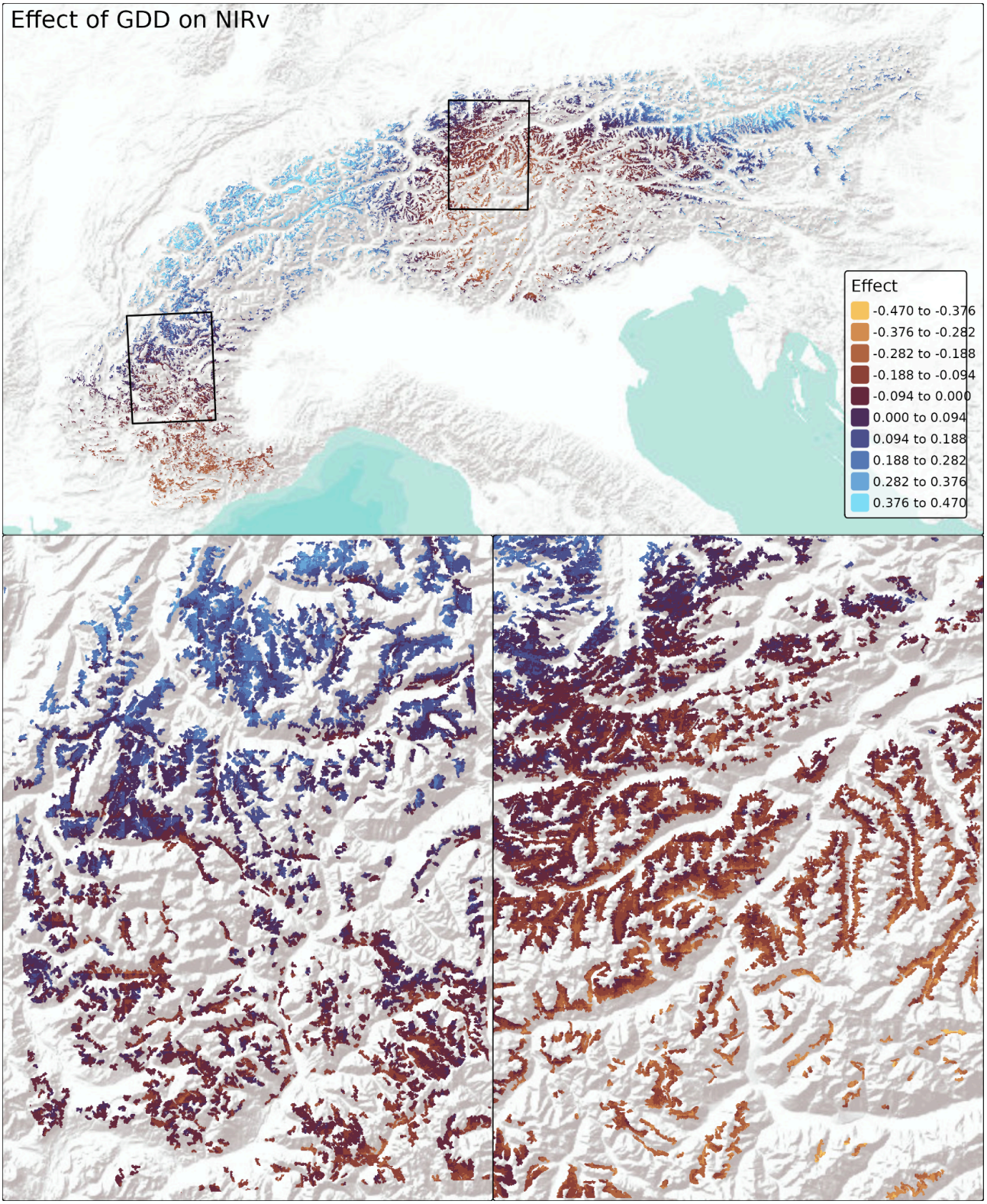

Figure 7. Predicted spatial distribution of the within-plot GDD→NIRv effect from the varying-coefficient LMM. Colors show the magnitude and direction of the GDD→NIRv effect on the *asinh* scale (blue = more negative; orange = more positive).

Discussion

By leveraging high-resolution remote sensing and causal inference, we showed that interannual variation in alpine grassland productivity can be confidently attributed to the interplay between direct climatic forcing and biodiversity-mediated climate-related processes, and that these effects are modulated by local environmental context.

Direct and indirect climatic effects on productivity

We found that warmer growing seasons had a negative effect on canopy chlorophyll content, photoprotective pigment investment, and canopy water status. These responses point to increasing physiological stress during warmer years, consistent with enhanced evaporative demand and soil moisture depletion (Vicca et al., 2016; Yuan et al., 2019). This pattern contradicts a purely energy-limited view in which warming uniformly enhances physiological investment. Instead, it aligns with the alternative prediction, that water limitation and heat stress dominate short term trait responses (Fig. S1). Greater winter snow accumulation increased canopy water content during subsequent growing seasons, consistent with earlier findings on reduced water limitation following delayed snowmelt and enhanced soil moisture recharge (Wipf & Rixen, 2010). Responses of canopy functional richness were weaker but aligned with expectations of the environmental filtering theory, with increased stress reducing the variation of functional strategies expressed (Chase & Leibold, 2009; Hawkins, 2003). This is also consistent with the trait driver theory, which predicts that shifts in trait means and dominance are expected to precede changes in trait diversity (Enquist et al., 2015).

Variation in canopy pigment-related traits had a positive effect on productivity, supporting mass-ratio expectations whereby dominant physiological strategies control ecosystem functioning (Enquist et al., 2015; Grime, 1998). Higher canopy chlorophyll content and lower relative photoprotective investment were consistently associated with higher productivity. Contrary to our expectations, we found a negative, although weak, effect of canopy water status on productivity, which may reflect energy–water co-limitation under cooler or cloudier conditions (Damm et al., 2018). Canopy functional richness had a consistently negative effect on vegetation productivity, indicating that years with broader expression of functional strategies tend to coincide with lower productivity. Rather than supporting a positive diversity–productivity relationship, this result is consistent with Trait Driver Theory (Fig. S1), which predicts directional selection toward phenotypes that maximize productivity under prevailing environmental constraints, often accompanied by reduced variance in the expressed trait distribution. In this perspective, years with higher functional richness may reflect a relaxation of dominance by highly productive phenotypes, leading to lower aggregate carbon assimilation (Enquist et al., 2015). In our study, interannual fluctuations in functional richness likely reflect physiological adjustment of individuals in response to climatic variability, rather than species turnover, because our analysis captures short-term (year-to-year) variability within fixed plots over an eight-year period, a timescale over which major compositional turnover is unlikely in long-lived alpine grassland communities. Over longer community assembly trajectories, however, complementarity and insurance effects may still enhance productivity, stability, and resilience, as demonstrated in classical biodiversity–ecosystem functioning experiments (Isbell et al., 2015; Loreau & de Mazancourt, 2013; Tilman et al., 2014).

Warmer growing seasons had a strong direct effect on annual vegetation productivity, while greater snow accumulation had a negative effect. These results directly support our prediction that ecosystem productivity in mountain grasslands is primarily constrained by cumulative energy availability and growing-season length, thus being independent of short-term trait reorganization. In such energy-limited systems, higher thermal accumulation has been found to enhance productivity by extending the seasonal

period suitable for carbon assimilation and high metabolic rates (Piao et al., 2011). In addition, greater snow accumulation tends to delay snowmelt leading to shorter effective growing season and thus lower annual productivity (Körner, 2021b; Wipf & Rixen, 2010).

Our structural equation models revealed that these processes operate through two concurrent pathways: a direct energy-driven pathway and an indirect pathway mediated by canopy functional structure. For temperature accumulation, negative indirect effects via reduced pigment investment contradicted, but did not outweigh, the positive direct effects of longer and warmer growing seasons, ultimately resulting in higher net productivity. This finding of partitioned direct and indirect effects closely mirrors our expectation, according to which climatic controls on ecosystem functioning operate alongside, and sometimes in opposition to, biodiversity-mediated pathways. The coexistence of these opposing mechanisms could explain why we found increased productivity during warmer years despite simultaneous evidence of physiological stress within the canopy. Together, this may indicate that primary productivity is governed by constraints on the cumulative amount of energy available across the year, rather than by physiological limitations alone (Del Grosso et al., 2008; Fatichi et al., 2019; Nemani et al., 2003; Stephenson, 1998). For climatic water deficit, the contradicting direct and indirect effects that we found largely cancelled each other out, resulting in weak net impacts on productivity. This mediation through functional richness was, however, weak compared to the mediation we uncovered through pigment-related properties, indicating that biodiversity-mediated climate effects primarily operate through physiological expression of dominant canopy strategies rather than short-term changes in functional breadth. Such decoupling between physiological condition and productivity suggests that short-term productivity gains under warmer conditions may thus come at the cost of reduced canopy functional integrity, potentially constraining the persistence of these gains under continued climate change (De Bello, 2021; Dee et al., 2023)**.**

Environmental modulation of causal effects. A key result of this study was the finding that climatic effects on vegetation were context-dependent. The strength and direction of causal relationships linking climate to vegetation traits, including links between climate and ecosystem functioning, varied substantially across environmental gradients (climate, soil, topography). Among the static variables, climatic moderators dominated over soil and topographic factors, confirming earlier findings that macro-climatic variability sets the primary constraints on both trait and productivity response across the Alps (Dee et al., 2023; van der Plas, 2019). In contrast, however, we found that the effects of canopy functional structure on ecosystem functioning were comparatively weakly modulated by environmental context. This indicates that biodiversity–functioning relationships showed limited short-term modulation by environment, suggesting that dominant trait mechanisms may override context-dependent complementarity effects at interannual timescales (Isbell et al., 2015; Loreau, 1998; van der Plas, 2019).

In the **H1 pathways (climate → biodiversity)**, we found the, on average, strongest modulation by mean annual temperature and long-term climatic water deficit, indicating that the physiological response of canopy pigments to warming depends on baseline climate conditions. In cooler, relatively moist and energy-limited regions, increases in growing-season thermal accumulation translated into a relaxation of photoprotective pigment investment relative to chlorophyll activity, consistent with reduced photoprotection requirements under favourable thermal and moisture conditions (Demmig-Adams & Adams, 1996). In contrast, in the warmer and more arid areas of the south-western Alps, the negative GDD → CCI relationship weakened or reversed, suggesting that warming in such environmental contexts tends to co-occur with water stress, maintaining or enhancing the need for photoprotection despite thermal gains, as found in earlier studies (Chaves et al., 2003; Corona-Lozada et al., 2019; Damm et al., 2018). Elevation further buffered warming effects, with sites at higher locations showing attenuated declines in photoprotective investment. This highlights the expected joint role of baseline climate and topoclimatic

constraints in shaping canopy physiological responses to interannual warming. In the **H2 pathways (biodiversity → functioning)**, environmental modulation was weak overall, implying that the relationships between spectral trait composition or diversity and productivity are relatively stable. This further suggests that biodiversity–functioning linkages may emerge from biotic composition mechanisms (e.g., complementarity or mass‑ratio effects) that are relatively insensitive to background climate (Isbell et al., 2015; Loreau, 1998; van der Plas, 2019). In the **H3 pathways (climate → functioning)**, the baseline climate emerged as a key moderator of productivity responses, with the positive effects of growing-season warming being strongest where long-term water availability was highest (Choler, 2023; Corona-Lozada et al., 2019). Where warming coincided with low precipitation, positive productivity responses were weak or negligible. This pattern highlights a non-linear, co-limiting control of productivity by energy availability and water supply, whereby temperature effects dominate under energy limitation but are increasingly constrained as water limitation intensifies (Badgley et al., 2017; Richardson et al., 2013).

Together, our results highlight a coherent picture in which the environment exerts hierarchical control of productivity in both time and space. Specifically, spatial variation in (macro)climate and local topography modulates both plant physiological responses and ecosystem productivity responses to interannual variability in climate. Together, these results underscore the importance of a broad "response diversity" at regional scales, whereby different environmental contexts and functional composition provide alternative pathways for ecosystem function -supporting responses to climatic forcing (Elmqvist et al., 2003; Seddon et al., 2016).

Perspectives and limits. Our findings highlight several directions for future research. First, the strong spatial variability in causal effect directions cautions against universal expectations of biodiversity–ecosystem functioning relationships, as biodiversity can buffer, amplify, or decouple climate impacts depending on the environmental context. Replicating this framework across other mountainous ecosystems will be critical for assessing the generality of these patterns. Second, extending analyses beyond productivity to ecosystem stability, resilience, and multifunctionality will help evaluate the long-term consequences of biodiversity change (De Bello, 2021; Isbell et al., 2015). Third, the comparatively weak and spatially stable biodiversity effects that we observed likely reflect the short temporal scope of our study and the omission of delayed biodiversity responses to climate. Incorporating lagged community and trait dynamics is therefore a key priority for further enhancing our understanding of long-term ecosystem resilience (Alexander et al., 2015, 2018; Dullinger et al., 2012). Fourth, climatic effects on productivity are likely non-linear, highlighting the need to explicitly consider thresholds and saturation effects under continued warming (Körner, 2021b). Finally, linking spectral proxies more directly to species-level trait databases, integrating belowground processes, and accounting for land-use and management drivers will be essential for developing comprehensive, policy-relevant causal maps of ecosystem responses to global change.

Conclusion. By integrating remote sensing and causal inference, our study bridges the gap between theory and application, offering a path toward predictive, spatially explicit ecology. By disentangling direct and biodiversity-mediated climate effects across environmental gradients, this study provides a spatially explicit framework to anticipate where productivity gains under warming are likely to persist and where physiological constraints may limit long-term ecosystem functioning. Ultimately, our framework lays the foundation for spatially explicit predictions of ecosystem trajectories, providing a causal lens to anticipate and manage the ecological consequences of climate change in mountain landscapes and elsewhere.

Data availability

All raw data used in this study are publicly available and were accessed and processed in Google Earth Engine (GEE). The spatial mask defining natural alpine grasslands above 1,000 m a.s.l. across the European Alps is available as a GEE asset at:
https://code.earthengine.google.com/?asset=users/pierregauzere/natural_grasslands_1000m_europe
The set of 10,000 randomly selected grassland plots (60 m radius buffers) used as units of analysis is available as a GEE vector asset at:
https://code.earthengine.google.com/?asset=users/pierregauzere/NatGrass_Alps_buffers60m_10000
Sentinel-2 Level-2A surface reflectance imagery (COPERNICUS/S2_SR_HARMONIZED), climate reanalysis products (ERA5-Land and TerraClimate), and static environmental layers (Copernicus DEM, WorldClim, OpenLandMap, HydroATLAS) are all publicly available datasets accessed directly within GEE.
All processing steps used to derive plot-level spectral traits (CIre, CCI, NDII), vegetation productivity (NIRv), interannual climate anomalies (GDD, CWD, SWE), and static environmental variables are fully documented and reproducible via the GEE scripts provided by the authors. The main scripts can be accessed and executed at the following links:
Script for computing spectral traits and productivity from Sentinel-2 imagery:
https://code.earthengine.google.com/045dff0eec966c841f443feb4bd1eb7c?accept_repo=users%2Fgisizw%2FGEE-PICX
Script for computing interannual climate time series (GDD, CWD, SWE):
https://code.earthengine.google.com/9e8314e07b23d0fab6fcc8eb3aaf83d2?accept_repo=users%2Fgisizw%2FGEE-PICX
Script for compiling static environmental variables:
https://code.earthengine.google.com/9e8314e07b23d0fab6fcc8eb3aaf83d2?accept_repo=users%2Fgisizw%2FGEE-PICX
All analyses were conducted using derived plot-level time series exported from GEE; no proprietary data were used. The full workflow therefore allows independent reproduction of all results starting from publicly available raw data.

References

Alexander, J. M., Chalmandrier, L., Lenoir, J., Burgess, T. I., Essl, F., Haider, S., Kueffer, C., McDougall, K., Milbau, A., Nuñez, M. A., Pauchard, A., Rabitsch, W., Rew, L. J., Sanders, N. J., & Pellissier, L. (2018). Lags in the response of mountain plant communities to climate change. *Global Change Biology*, *24*(2), 563–579.

Alexander, J. M., Diez, J. M., & Levine, J. M. (2015). Novel competitors shape species' responses to climate change. *Nature*, *525*(7570), 515–518.

Badgley, G., Field, C. B., & Berry, J. A. (2017). Canopy near-infrared reflectance and terrestrial photosynthesis. *Science Advances*, *3*(3), e1602244.

Cavender-Bares, J., Gamon, J., & Hobbie, S. E. (2022). Remote sensing of plant biodiversity. *Annual Review of Environment and Resources*, *47*, 337–365.

Cavender-Bares, J., Schneider, F. D., Santos, M. J., Armstrong, A., Carnaval, A., Dahlin, K. M., Fatoyinbo, L., Hurtt, G. C., Schimel, D., Townsend, P. A., Ustin, S. L., Wang, Z., & Wilson, A. M. (2022). Integrating remote sensing with ecology and evolution to advance biodiversity conservation. *Nature Ecology & Evolution*, *6*(5), 506–519.

Chapin, F. S., 3rd, Zavaleta, E. S., Eviner, V. T., Naylor, R. L., Vitousek, P. M., Reynolds, H. L., Hooper, D. U., Lavorel, S., Sala, O. E., Hobbie, S. E., Mack, M. C., & Díaz, S. (2000). Consequences of changing biodiversity. *Nature*, *405*(6783), 234–242.

Chase, J. M., & Leibold, M. A. (2009). *Ecological niches: linking classical and contemporary approaches*. https://www.academia.edu/download/51130686/j.biocon.2004.02.00320161231-14998-9f59tq.pdf

Chaves, M. M., Maroco, J. P., & Pereira, J. S. (2003). Understanding plant responses to drought-From genes to the whole plant. *Functional Plant Biology*, *30*, 239–264.

Choler, P. (2023). Above-treeline ecosystems facing drought: lessons from the 2022 European summer heat wave. *Biogeosciences*, *20*(20), 4259–4272.

Corona-Lozada, M. C., Morin, S., & Choler, P. (2019). Drought offsets the positive effect of summer heat waves on the canopy greenness of mountain grasslands. *Agricultural and Forest Meteorology*, *276-277*(107617), 107617.

Damm, A., Paul-Limoges, E., Haghighi, E., Simmer, C., Morsdorf, F., Schneider, F. D., van der Tol, C., Migliavacca, M., & Rascher, U. (2018). Remote sensing of plant-water relations: An overview and future perspectives. *Journal of Plant Physiology*, *227*, 3–19.

De Bello, F. (2021). Towards a theory of functional biodiversity dynamics. *Trends in Ecology & Evolution*, *36*, 812–823.

Dee, L. E., Ferraro, P. J., Severen, C. N., Kimmel, K. A., Borer, E. T., Byrnes, J. E. K., Clark, A. T., Hautier, Y., Hector, A., Raynaud, X., Reich, P. B., Wright, A. J., Arnillas, C. A., Davies, K. F., MacDougall, A., Mori, A. S., Smith, M. D., Adler, P. B., Bakker, J. D., … Loreau, M. (2023). Clarifying the effect of biodiversity on productivity in natural ecosystems with longitudinal data and methods for causal inference. *Nature Communications*, *14*(1), 2607.

Del Grosso, S., Parton, W., Stohlgren, T., Zheng, D., Bachelet, D., Prince, S., Hibbard, K., & Olson, R. (2008). Global potential net primary production predicted from vegetation class, precipitation, and temperature. *Ecology*, *89*(8), 2117–2126.

Demmig-Adams, B., & Adams, W. W., III. (1996). Xanthophyll cycle and light stress in nature: uniform response to excess direct sunlight among higher plant species. *Planta*, *198*(3), 460–470.

Denissen, J. M. C., Teuling, A. J., Pitman, A. J., Koirala, S., Migliavacca, M., Li, W., Reichstein, M., Winkler, A. J., Zhan, C., & Orth, R. (2022). Widespread shift from ecosystem energy to water limitation with climate change. *Nature Climate Change*, *12*(7), 677–684.

Dullinger, S., Gattringer, A., Thuiller, W., Moser, D., Zimmermann, N. E., Guisan, A., Willner, W., Plutzar, C., Leitner, M., Mang, T., Caccianiga, M., Dirnböck, T., Ertl, S., Fischer, A., Lenoir, J., Svenning, J.-C., Psomas, A., Schmatz, D. R., Silc, U., … Hülber, K. (2012). Extinction debt of high-mountain plants under twenty-first-century climate change. *Nature Climate Change*, *2*(8), 619–622.

Elmqvist, T., Folke, C., Nyström, M., Peterson, G., Bengtsson, J., Walker, B., & Norberg, J. (2003). Response diversity, ecosystem change, and resilience. *Frontiers in Ecology and the Environment*, *1*(9), 488–494.

Enquist, B. J., Norberg, J., Bonser, S. P., Violle, C., Webb, C. T., Henderson, A., Sloat, L. L., & Savage, V. M. (2015). Chapter Nine - Scaling from Traits to Ecosystems: Developing a General Trait Driver Theory via

Integrating Trait-Based and Metabolic Scaling Theories. In S. Pawar, G. Woodward, & A. I. Dell (Eds.), *Advances in Ecological Research* (Vol. 52, pp. 249–318). Academic Press.

Fatichi, S., Pappas, C., Zscheischler, J., & Leuzinger, S. (2019). Modelling carbon sources and sinks in terrestrial vegetation. *The New Phytologist*, *221*(2), 652–668.

Gamon, J. A., Somers, B., Malenovský, Z., Middleton, E. M., Rascher, U., & Schaepman, M. E. (2019). Assessing vegetation function with imaging spectroscopy. *Surveys in Geophysics*, *40*(3), 489–513.

Grime, J. P. (1998). Benefits of plant diversity to ecosystems: immediate, filter and founder effects. *The Journal of Ecology*, *86*(6), 902–910.

Hawkins. (2003). Energy, water, and broad-scale geographic patterns of species richness. *Ecology*, *84*(12), 3105–3117.

Isbell, F., Craven, D., Connolly, J., Loreau, M., Schmid, B., Beierkuhnlein, C., Bezemer, T. M., Bonin, C., Bruelheide, H., de Luca, E., Ebeling, A., Griffin, J. N., Guo, Q., Hautier, Y., Hector, A., Jentsch, A., Kreyling, J., Lanta, V., Manning, P., … Eisenhauer, N. (2015). Biodiversity increases the resistance of ecosystem productivity to climate extremes. *Nature*, *526*(7574), 574–577.

Körner, C. (2021a). *Alpine Plant Life: Functional Plant Ecology of High Mountain Ecosystems*. Springer Nature.

Körner, C. (2021b). Plant ecology at high elevations. In *Alpine Plant Life* (pp. 1–22). Springer International Publishing.

Lavorel, S., & Garnier, E. (2002). Predicting changes in community composition and ecosystem functioning from plant traits: revisiting the Holy Grail. *Functional Ecology*, *16*(5), 545–556.

Leibold, M. A., Chase, J. M., & Ernest, S. K. M. (2017). Community assembly and the functioning of ecosystems: how metacommunity processes alter ecosystems attributes. *Ecology*, *98*(4), 909–919.

Loreau, M. (1998). Biodiversity and ecosystem functioning: a mechanistic model. *Proceedings of the National Academy of Sciences of the United States of America*, *95*(10), 5632–5636.

Loreau, M., & de Mazancourt, C. (2013). Biodiversity and ecosystem stability: a synthesis of underlying mechanisms. *Ecology Letters*, *16 Suppl 1*, 106–115.

Loreau, M., & Hector, A. (2001). Partitioning selection and complementarity in biodiversity experiments. *Nature*, *412*(6842), 72–76.

Mod, H. K., Scherrer, D., Luoto, M., & Guisan, A. (2016). What we use is not what we know: environmental predictors in plant distribution models. *Journal of Vegetation Science: Official Organ of the International Association for Vegetation Science*, *27*(6), 1308–1322.

Nemani, R. R., Keeling, C. D., Hashimoto, H., Jolly, W. M., Piper, S. C., Tucker, C. J., Myneni, R. B., & Running, S. W. (2003). Climate-driven increases in global terrestrial net primary production from 1982 to 1999. *Science (New York, N.Y.)*, *300*(5625), 1560–1563.

Piao, S., Wang, X., Ciais, P., Zhu, B., Wang, T., & Liu, J. (2011). Changes in satellite-derived vegetation growth trend in temperate and boreal Eurasia from 1982 to 2006: CHANGE IN VEGETATION GROWTH OVER EURASIA. *Global Change Biology*, *17*(10), 3228–3239.

Richardson, A. D., Keenan, T. F., Migliavacca, M., Ryu, Y., Sonnentag, O., & Toomey, M. (2013). Climate change, phenology, and phenological control of vegetation feedbacks to the climate system. *Agricultural and Forest Meteorology*, *169*, 156–173.

Saugier, B. (2001). Plant strategies, vegetation processes, and ecosystem properties. *Plant Science: An International Journal of Experimental Plant Biology*, *161*(4), 813.

Seddon, A. W. R., Macias-Fauria, M., Long, P. R., Benz, D., & Willis, K. J. (2016). Sensitivity of global terrestrial ecosystems to climate variability. *Nature*, *531*(7593), 229–232.

Stephenson, N. (1998). Actual evapotranspiration and deficit: biologically meaningful correlates of vegetation distribution across spatial scales. *Journal of Biogeography*, *25*(5), 855–870.

Suding, K. N., Lavorel, S., Chapin, F. S., III, Cornelissen, J. H. C., Díaz, S., Garnier, E., Goldberg, D., Hooper, D. U., Jackson, S. T., & Navas, M.-L. (2008). Scaling environmental change through the community-level: a trait-based response-and-effect framework for plants. *Global Change Biology*, *14*(5), 1125–1140.

Tilman, D., Isbell, F., & Cowles, J. M. (2014). Biodiversity and Ecosystem Functioning. *Annual Review of Ecology, Evolution, and Systematics*, *45*(1), 471–493.

Ustin, S. L., & Gamon, J. A. (2010). Remote sensing of plant functional types. *The New Phytologist*, *186*(4), 795–816.

Ustin, S. L., Gitelson, A. A., Jacquemoud, S., Schaepman, M., Asner, G. P., Gamon, J. A., & Zarco-Tejada, P. (2009). Retrieval of foliar information about plant pigment systems from high resolution spectroscopy.

Remote Sensing of Environment, *113*, S67–S77.

Van Cleemput, E., Adler, P. B., Suding, K. N., Rebelo, A. J., Poulter, B., & Dee, L. E. (2024). Scaling-up ecological understanding with remote sensing and causal inference. *Trends in Ecology & Evolution*. https://doi.org/10.1016/j.tree.2024.09.006

van der Plas, F. (2019). Biodiversity and ecosystem functioning in naturally assembled communities. *Biological Reviews of the Cambridge Philosophical Society*, *94*(4), 1220–1245.

Vicca, S., Balzarolo, M., Filella, I., Granier, A., Herbst, M., Knohl, A., Longdoz, B., Mund, M., Nagy, Z., Pintér, K., Rambal, S., Verbesselt, J., Verger, A., Zeileis, A., Zhang, C., & Peñuelas, J. (2016). Remotely-sensed detection of effects of extreme droughts on gross primary production. *Scientific Reports*, *6*(1), 28269.

Wipf, S., & Rixen, C. (2010). A review of snow manipulation experiments in Arctic and alpine tundra ecosystems. *Polar Research*, *29*(1).

Yuan, W., Zheng, Y., Piao, S., Ciais, P., Lombardozzi, D., Wang, Y., Ryu, Y., Chen, G., Dong, W., Hu, Z., Jain, A. K., Jiang, C., Kato, E., Li, S., Lienert, S., Liu, S., Nabel, J. E. M. S., Qin, Z., Quine, T., … Yang, S. (2019). Increased atmospheric vapor pressure deficit reduces global vegetation growth. *Science Advances*, *5*(8), eaax1396.

Supporting Information

S1 — Mechanistic expectations underlying hypotheses H1–H4

H1 — Climate→ Biodiversity (spectral traits and diversity).
Growing-season thermal accumulation (GDD) increase chlorophyll investment (↑CIre) and reduce photoprotective demand (↑CCI) because more favorable growing seasons relaxes thermal constraints, allowing plants to invest more in photosynthetic pigments and reduce relative photoprotective pigment ratios. Alternatively , if high GDD coincides with water limitation and heat stress, it can decrease chlorophyll (↓CIre) and increase photoprotective demand (↓CCI). Higher growing-season water deficits (CWD) lower leaf water content and pigment maintenance (↓NDII, ↓CIre; ↓CCI via higher carotenoid fractions).
More snow during the winter (SWE) leading to late snowmelt reduces the window for chlorophyll pigment gain (↑CIre) but decreases frost risk (Körner, 2021b; Wipf & Rixen, 2010). Alternatively, if water limitation dominates, extra heat and less snow reduce the amount of pigments and increase water deficit (↓CIre, ↓CCI, ↓NDII) despite longer growing seasons. From a Trait Driver Theory perspective, these expectations arise because climatic anomalies act as environmental filters that shift the distribution of expressed physiological traits at the community level, either through changes in dominance or within-species physiological adjustment **(Violle et al., 2007; Enquist et al., 2015).**
Spectral trait diversity (FRic) increases if climate interannual variability leads to idiosyncratic responses of species, and decreases under environmental filtering of species negatively affected by strong climate anomalies (Chase & Leibold, 2009; Hawkins, 2003). Alternatively, FRic remains stable if community reassembly dynamics causes lags in physiological adjustment. Under Trait Driver Theory, such diversity responses are expected to be secondary to shifts in trait distributions: strong climatic filtering should primarily alter trait means and dominance patterns, with trait diversity responding only when species turnover or asynchronous responses are sufficiently strong (Enquist et al., 2015; Enquist et al., 2020).

H2 — Biodiversity → Functioning.
CIre/CCI/NDII primarily reflect mass-ratio control via dominant canopy strategies, whereas FRic is the metric most closely aligned with complementarity/insurance expectations at interannual scales. Higher chlorophyll-related reflectance (↑CIre) and lower photoprotective demand (↑CCI) increases seasonal productivity (↑NIRv), while higher canopy water content (↑NDII) supports higher productivity when energy supply is sufficient (Grime, 1998; Loreau & Hector, 2001). Trait Driver Theory explicitly predicts that ecosystem functioning should scale with the abundance-weighted distribution of functional traits expressed in the canopy, rather than with species or trait richness per se **(Enquist et al., 2007; Enquist et al., 2015; Shipley et al., 2016)**. Thus, strong links between pigment- and water-related spectral traits and productivity are expected. Higher spectral trait diversity (FRic) is considered to favour productivity because functionally distinct strategies partition resources (complementary effect) and respond asynchronously to climate. This can promote more complete and temporally stable use of light and water. Alternatively, at interannual scales, diversity effects could be weak or even negative if trait changes reflect stress responses that dilute the dominance of species that efficiently convert absorbed light into carbon (Loreau & de Mazancourt, 2013). In wet or cool years NDII could rise while NIRv falls if radiation limits photosynthesis. Under Trait Driver Theory, such weak or negative diversity–productivity relationships are expected when increases in trait diversity arise from the inclusion of stress-tolerant or low-biomass strategies that contribute little to fluxes, even though they increase functional space occupancy (**Enquist et al., 2015; Enquist et al., 2020).**

H3 — Climate → Functioning.
Expectation: higher GDD will directly increase productivity reflecting the extended and warmer growing season (↑NIRv), whereas higher growing-season water deficit (CWD) should decrease productivity (↓NIRv). Higher snow winter equivalent (SWE) can decrease productivity when decreasing season length (later snowmelt) is not offset by frost or higher evaporative demand (Körner, 2021a; Wipf & Rixen, 2010). Alternatively, in warm years with drought may result in muted or neutral net effects in functioning if water stress cancels out the benefits of energy gains. These direct effects correspond to climatic controls acting on ecosystem-level fluxes independently of community trait reorganization, reflecting constraints on energy input and carbon assimilation rather than shifts in trait distributions

H4 — Environmental control and spatial prediction.

Background environmental conditions modulate the effects of H1-3. Our main expectation in H1 (climate→biodiversity effects), is that the response of spectral traits to climate anomalies should be modulated across large scales based on climatic baseline conditions. Subsequently, at smaller spatial scales, topography and soil are also expected to modulate the response, as insolation and soil water retention capacity can intensify or mitigate pigment content and water stress. Trait Driver Theory predicts that the sensitivity of trait distributions to climatic anomalies should vary systematically along environmental gradients, as baseline conditions determine both the pool of viable strategies and the strength of environmental filtering. Our main expectation for H2 (biodiversity→productivity effects), is that positive links exist between chlorophyll-related composition (CIre, higher CCI) and NIRv, and that these are strongest in high moisture areas with high insolation. Thus, diversity–productivity effects (FRic→NIRv) could weaken under more stressful environmental conditions (coldest or driest) due to strong environmental filtering, but could also turn positive if harsher environments (cold, dry) promote positive interactions and greater niche differentiation. Our main expectation for H3 (climate→productivity effects), is that in wetter and lower insolation contexts warming benefits on NIRv should be amplified, whereas high elevation, cold, snow-dominated, or highly insolated sites with coarse/alkaline soils should shift responses toward stress-limited regimes and thus attenuate warming benefits.

S2 - Pair plots of vegetation indices

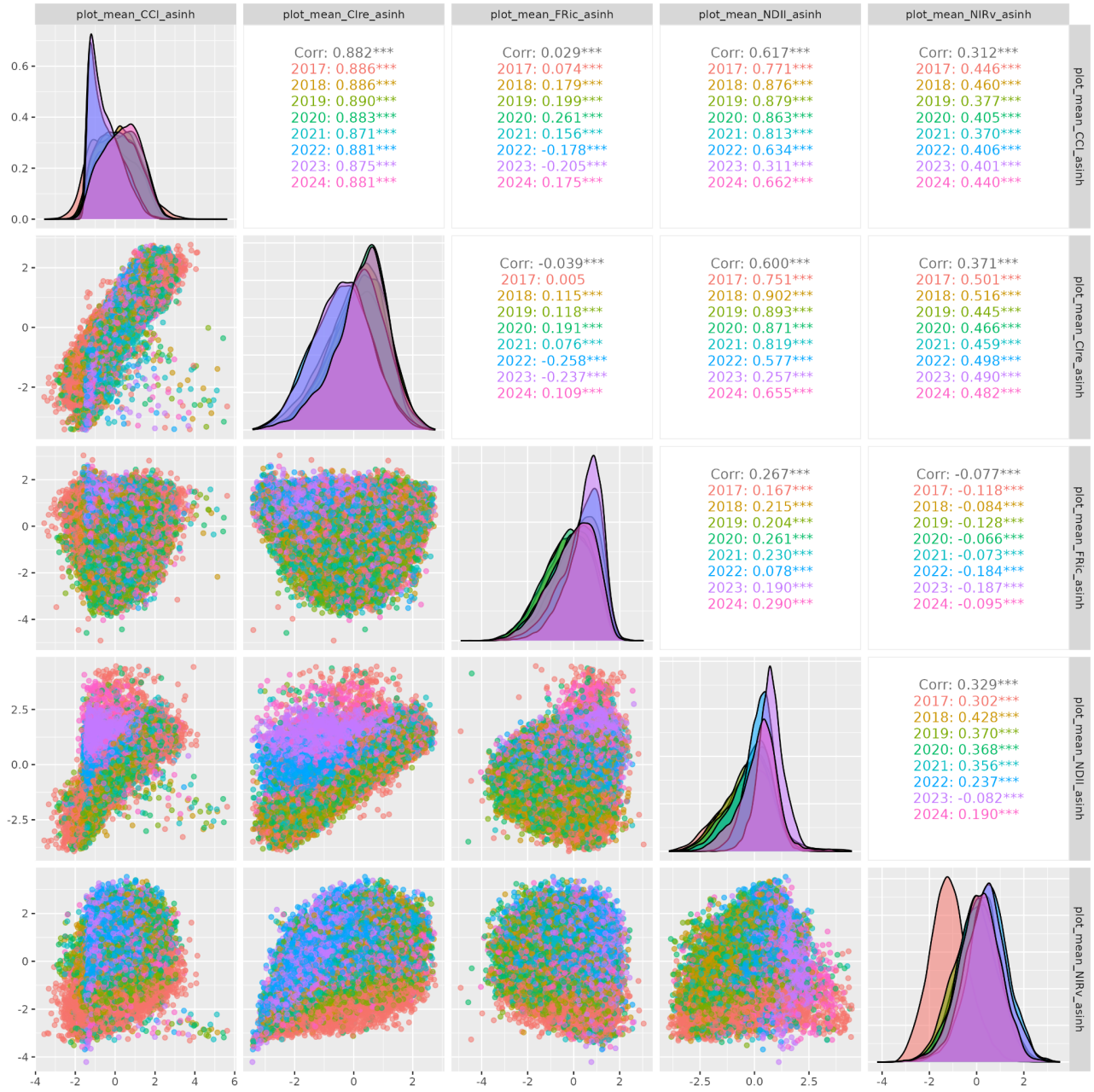

The observed covariance among spectral indices and productivity is consistent with climate acting on integrated canopy properties (leaf area, pigment investment, structure) that simultaneously regulate light absorption and carbon uptake, rather than on independent trait dimensions

S3 - Extended Methods

This section provides the full technical description of data sources, preprocessing workflows, statistical models, and robustness analyses underlying the main-text Methods, which are presented in a condensed form for clarity. Note that all the scripts to generate the data are available directly on Google earth engine, see data availability for the links.

Data and processing

Remotely sensed vegetation time series

We used Sentinel-2 Level-2A surface reflectance imagery (10–20 m spatial resolution) from the COPERNICUS/S2_SR_HARMONIZED collection. All processing was conducted in Google Earth Engine. For each year between 2017 and 2024, imagery was restricted to the growing season (April–October). Cloud and cirrus contamination were masked using QA60 bits 10 and 11, and snow and ice were removed using the Scene Classification Layer (SCL = 11).

To ensure reliable estimation of spectral indices in alpine environments, pixels with low vegetation signal were excluded prior to index computation. Specifically, pixels with fractional vegetation cover below 0.6 were filtered out, thereby minimizing contamination from bare ground, rocks, senescent litter, or mixed surfaces known to bias pigment- and water-related indices. Surface reflectance bands (B1–B12) were scaled to unitless reflectance and constrained to the [0, 1] interval.

All retained pixels within each 60 m-radius plot were processed independently prior to spatial aggregation.

Spectral traits as proxies of realised canopy functional structure. We used three spectral indices to characterize canopy functional structure: a red-edge chlorophyll index (CIre), a carotenoid–chlorophyll index (CCI), and a near-infrared water index (NDII). These indices reflect complementary aspects of plant physiological functioning, including pigment investment, photoprotective demand, and canopy water status. The estimated spectral traits function as proxies for three key leaf-level physiological traits that capture complementary aspects of vegetation functioning: photosynthetic capacity, photoprotection, and leaf water status (Gitelson et al., 2006). More precisely, CIre is a proxy for leaf chlorophyll content, with higher CIre values indicating greater chlorophyll content and higher potential photosynthetic activity (Ali et al., 2020; Croft et al., 2017); CCi is a proxy for leaf carotenoid content, and reflects investment in photoprotective pigments and stress-response capacity (Lichtenthaler et al., 2007); NDII is a proxy for leaf water content, and reflects plant water status and strategies of water use and its conservation. Although indirect, this set of spectral traits have the advantage of being ecologically complementary (Schneider et al., 2017), providing independent information about photosynthetic, photoprotective, and water-use strategies (Damm et al., 2018). Rather than interpreting them as direct measurements of species composition, we treat these indices as proxies of realised canopy functional structure, integrating both changes in species dominance and within-species physiological adjustment to interannual climatic variability. Because these indices capture expressed canopy properties, variation in CIre, CCI, and NDII can arise from multiple processes operating simultaneously, including shifts in species relative abundance (mass-ratio effects) and phenotypic or physiological plasticity within species. Consequently, biodiversity-mediated effects estimated in our causal framework should be interpreted as operating through changes in canopy functional structure, rather than taxonomic turnover alone.

Three spectral indices were derived to characterize canopy pigment investment and water status:

- **Red-Edge Chlorophyll Index (CIre)**

$$CIre = \frac{B7}{B5} - 1$$

following Clevers and Gitelson (2013), using Sentinel-2 red-edge bands B5 and B7.

- **Carotenoid-to-Chlorophyll Index (CCI)**

  $$CCI = \frac{B3 - B4}{B3 + B4}$$

  following Gamon et al. (2019) and Helfenstein et al. (2022), based on visible bands B3 and B4.

- **Normalized Difference Infrared Index (NDII)**

  $$NDII = \frac{B8A - B11}{B8A + B11}$$

  following Hardisky et al. (1983), using near-infrared (B8A) and short-wave infrared (B11) bands.

To summarize the seasonal physiological state while reducing residual noise from clouds, view angle effects, or short-term phenological fluctuations, CIre, CCI, and NDII were composited using the 80th percentile of all valid observations within each growing season and plot. This percentile-based compositing targets near-peak physiological conditions while avoiding extreme outliers.

CIre, CCI, and NDII quantify canopy-level pigment investment and water status derived from reflected radiation and are therefore treated as indicators of realised canopy functional structure rather than as direct measurements of species composition. Variation in these indices may arise from changes in species relative abundance or identity as well as from within-species physiological or phenotypic adjustment to interannual climatic conditions. Because canopy biophysical properties (e.g. leaf area, pigment pools, and structure) jointly influence multiple spectral bands, CIre, CCI, NDII, and productivity metrics are expected to covary at the plot scale. In the causal framework used here, this shared variance is interpreted as a meaningful signal associated with canopy functional structure rather than as a redundant radiometric artefact (see Figure S2 for pairwise relationships among indices).

Vegetation productivity

Vegetation productivity was quantified using near-infrared reflectance of vegetation (NIRv), following Badgley et al. (2017):

$$NIRv = \left(\frac{B8 - B4}{B8 + B4}\right) \times B8$$

where B8 and B4 correspond to Sentinel-2 near-infrared and red bands, respectively. NIRv provides a linear proxy of gross primary productivity across a wide range of ecosystems and is particularly robust when integrated over time.

To estimate cumulative growing-season productivity, NIRv was computed for each valid Sentinel-2 acquisition between April and October and summed across the season for each pixel. All 10 m pixels within each 60 m-radius plot were retained, and pixel-level values were exported for each plot–year combination. This procedure leverages the high revisit frequency of Sentinel-2 (≈5 days) to approximate seasonal integration of canopy carbon uptake while minimizing contamination from clouds and snow. **NIRv** provides a linear proxy for gross primary production (GPP) in most ecosystems, and is particularly reliable when integrated over the growing season (Yu et al., 2024; Zheng et al., 2024). The resulting dataset provides, for each plot and year, (i) near-peak estimates of canopy pigment and water-status traits and (ii) an integrated metric of growing-season productivity suitable for subsequent plot-level causal analyses.

Interpretation of spectral mediators. The indices CIre, CCI, and NDII reflect canopy-level pigment investment and water status, and are therefore treated here as metrics of realised canopy functional structure rather than direct measurements of taxonomic or trait composition. Variation in these indices can arise from (i) changes in species' relative abundances and identities (mass-ratio–type shifts), and/or (ii) within-species phenotypic and physiological adjustment to interannual conditions. Consequently, indirect (mediated) effects estimated in our piecewise SEM should be interpreted as operating through changes in canopy functional structure (trait expression), not necessarily through compositional turnover alone. Because canopy biophysical properties jointly influence multiple spectral bands, these indices are expected to covary at a plot scale (Figure S2). In our causal framework, this shared variance is interpreted as meaningful canopy functional structure rather than treated as redundant radiometric noise.

Climate interannual variability

We characterized interannual climatic variability using three variables selected to represent the primary abiotic constraints on mountain grassland functioning: thermal energy availability, water limitation, and snow dynamics. These variables were chosen based on well-established theoretical and empirical links between climate, plant physiological activity, and growing-season length in mountain ecosystems (Körner, 2021b; Stephenson, 1998; Wipf & Rixen, 2010).

Thermal conditions were quantified using growing degree days above 5 °C (GDD), which integrates both temperature magnitude and growing-season duration and is a standard proxy for thermal energy available for plant growth. Water limitation was characterized using growing-season climatic water deficit (CWD), which captures the balance between atmospheric demand and water supply and has been shown to be a key determinant of plant stress and productivity. Snow dynamics were represented by maximum winter snow water equivalent (SWE), reflecting the role of snowpack in regulating soil moisture recharge, frost protection, and the timing of snowmelt and growing-season onset.

Climate time series were extracted for each plot for the period 2017–2024 from gridded reanalysis and climatological datasets (ERA5-Land hourly reanalysis at 9km resolution for GDD, TerraClimate monthly fields at ~4km for CWD and SWE). Although the native spatial resolution of these products is coarser than the plot scale, our inference targets within-plot interannual anomalies rather than fine-scale spatial gradients. Consequently, climate variables are interpreted as year-to-year deviations experienced by each plot relative to its own mean climatic context, rather than as precise microclimatic estimates. This approach is appropriate for isolating temporal climatic forcing while controlling for persistent spatial differences among sites.

Static environmental variables

To characterize the background environmental context in which interannual climate variability operates, we compiled a set of **static environmental variables** describing long-term climatic conditions, soil properties, and topography across the entire study area. We retained a theory-driven, low-collinearity set of variables for analyses including climatic, soil, and topographic descriptors. The static climatic descriptors that were retained were Climatic Water Deficit (CWD, mm), Mean Annual Precipitation (MAP, mm), Mean Annual Temperature (MAT, °C, lapse rate downscaled at 100m), SWE (mm), and Temperature seasonality extracted from WorldClim BIO layers (BIO1 for annual mean temperature, BIO4 for temperature seasonality, BIO12 for annual precipitation), and TerraClimate monthly fields to obtain the mean annual climatic water deficit (CWD) over 2001–2020, and the snow water equivalent baseline as the mean, across years, of the hydrologic-winter (October of year y–1 to May of year y) maximum of monthly snow winter equivalent. The static soil descriptors that we retained were lithology, pH, sand percentage, and soil organic content. Lithology was assessed by rasterizing the HydroATLAS (GLiM-derived) majority lithology class to 100 m. pH,

sand percentage, and soil organic content were obtained from OpenLandMap (v02/v01) at 250 m resolution and depth-weighted to 0–30 cm (0–10 and 10–30 cm layers). The topographic predictors that we retained were Heat Load Index (HLI), mean elevation, and elevation range, computed from Copernicus Digital Elevation Model at 30 m resolution (Copernicus GLO-30). Mean elevation and elevation range were both aggregated from 30 m to 100 m resolution. HLI was computed by McCune–Keon formulation using slope, aspect (at 30 m resolution), and latitude, then aggregated at 100 m resolution. All static variables were harmonized on a common spatial grid harmonized on a continuous 100 m grid (EPSG:3035) covering the grassland mask (study area) and processed with consistent projections to avoid projection artifacts.

Analyses

Study design and variables.

We quantified how climate anomalies in a given year affect realised canopy functional structure and, in turn, ecosystem productivity in the same year across our panel of 10,000 Alpine grassland plots. For **Climate → Biodiversity (H1)**, the outcomes (i.e, response variables) were spectral trait composition (CCI, CIre, NDII), and diversity (FRic), while the treatments (i.e, explanatory variables) were climate anomalies of GGD5, CWD, and SWE. For **Biodiversity → Functioning (H2)**, the outcome was ecosystem productivity (NIRv), while the treatments were spectral indices of canopy functional structure (CCI, CIre, NDII, FRic). For **Climate → Functioning (H3)**, the outcome was ecosystem productivity (NIRv), the treatments were climate anomalies of GGD5, CWD, and SWE, and the mediators were spectral trait composition (CCI, CIre, NDII) and diversity (FRic).

Pre-processing and statistical models.

To target within-plot, year-to-year effects, we formed demeaned versions of time-varying variables by subtracting each plot's mean from the annual value (Mundlak/within–between decomposition). We then applied an inverse hyperbolic sine (*asinh*) transformation, where $\text{asinh}(x) = \ln(x + \text{sqrt}(x^2+1))$. Analyzing outcomes and treatments on the *asinh* scale provides the benefits of a log transformation without the limitations that a log transformation brings with it. Like a log transformation, *asinh* compresses skewness and makes multiplicative effects more linear and homoscedastic. Unlike the log transformation, however, it has the advantage of being defined at zero and for negative values, hence being applicable to anomalies without dropping or shifting observations. Finally, we performed linear mixed models (LMMs, using REML; lme4/lmerTest R packages) on transformed anomalies, including a random intercept for plot to capture time-invariant site heterogeneity and year fixed effects (factor) to absorb space-invariant temporal shocks (Wooldridge, 2002).

Estimand and identification.

Our core estimand was the within-plot effect of a given climate anomaly (or mediator) on the outcome in the same year, net of plot-invariant differences and shared year shocks. The plot random intercept (or plot fixed effect in the TWFE check, see below) removes all time-invariant confounding among plots (e.g., persistent soils, topography, long-term management differences), while the year fixed effects absorb any Alps-wide shocks common to all plots in a given year (e.g., sensor-wide artifacts, pan-Alpine anomalies not captured by the focal driver). The identification therefore assumed that remaining time-varying within-plot confounders were adequately controlled by our covariate set and that reverse causality was negligible at the annual aggregation used here.

As a robustness check, and to ensure the modelling approach was coherent with estimation based on a different modelling approach, we re-estimated our core mixed-effects models using a two-way fixed-effects

(TWFE) approach. For each hypothesis, we fit linear regressions with plot and year as fixed effects to isolate within-plot and year-to-year variation (the same estimand targeted by the LMMs). We used the same variables and transformations (on the *asinh* scale) and the same set of controls, meaning that point estimates were directly comparable. Uncertainty was computed using cluster-robust standard errors at the plot level. We implemented two-way fixed-effects with fixest::feols (Imai and Kim 2021), absorbing plot and year effects and extracting the coefficients for the same drivers and mediators as in the LMMs. The results of the TWFE models closely matched the LMM within-effects, providing support for our conclusions not depending on the modelling framework but reflecting stable, within-plot relationships (Fig.S4).

We addressed three questions with the linear mixed models. For **H1 (Climate → Biodiversity)** we performed one LMM per biodiversity variable. For **H2 (Biodiversity → Productivity)** we performed one LMM for NIRv on biodiversity mediators. Finally, for **H3 (Climate + Biodiversity → Productivity)** we fitted one LMM for NIRv on climate anomalies and biodiversity mediators. Within-plot effects were coefficients for demeaned predictors (i.e., temporal anomalies on each plot) interpreted as expected change in the response when a predictor deviated from its plot mean. For moderate to large magnitudes, *asinh(y)* behaves very much like *log(y)*, so coefficients can be read approximately as semi-elasticities (percent-type changes), while when close to zero, it behaves linearly, thus preserving information where values are small.

Piecewise structural equation modeling (SEM).
To separate direct climatic effects on productivity from indirect effects that operate through the canopy functional structure (i.e "biodiversity" metrics), we linked our fitted LMMs into a simple, piecewise SEM. First, for each biodiversity metric we used the climate→biodiversity models (our "H1" set) to quantify how a given climate anomaly changes canopy functional structure (CIre, CCI, NDII) or functional richness (FRic). Second, we used the productivity model (our "H3" set) that includes both climate and biodiversity to quantify how those biodiversity changes translate into changes in NIRv, while also estimating the remaining (direct) effect of climate on NIRv after holding canopy functional structure constant (Fig. 1).

For each climate driver, the direct effect was captured by the coefficient of that driver in the productivity model that includes biodiversity. The indirect effect was the product of two effects: the effect of climate on a given biodiversity metric, and the effect of that biodiversity metric on NIRv. We computed this for each biodiversity pathway and then summed them to obtain the total indirect effect. The total climate effect on productivity was the sum of the direct effect and all indirect effects. To assess statistical uncertainty, we drew repeatedly from the joint (approximately normal) distribution of the fixed effects in the fitted models and recomputed the direct, indirect, and total effects.

Spatially explicit varying-coefficient LMMs.
To quantify how the within-plot effect of each climatic driver varied across the study area, we fitted a varying coefficient linear mixed model for each main causal effect retained in the SEM (see the analysis workflow Figure 3). Here, the within-plot effect of treatment on outcome is allowed to change linearly with the static environment by adding interaction terms with static moderators (here: topography, soils, climate). Each moderator is standardized (mean zero, unit variance across the training plots) to make coefficients comparable and to define a clear reference environment (here: the mean of the plots). The mixed-model backbone stays identical to the main LMMs (here: the random intercept for plot and year), meaning that the varying-coefficient model remained directly comparable to the previous models.

Spatial maps of the local effects.
After fitting a varying-coefficient model, we computed, for every pixel, the within-plot, slope of the outcome with respect to the driver. This value equals the baseline within-plot slope (evaluated at the

average environment of the training plots) plus the linear adjustments that the standardized static moderators at that pixel contribute with. We retained only pixels where the standardized static moderator values fell within the range observed across training plots. This prevented including model predictions in environmental conditions that were not represented in the data. To represent parameter uncertainty in the mapped effects, we sampled from the coefficients' estimated multivariate normal distribution (using the model's coefficient covariance), recomputed the local slope for each draw, and summarized across draws to obtain a mean effect map and a standard-deviation map. These reflect uncertainty in the estimated coefficients, conditional on the random-effects structure and the moderator rasters.

Each mapped value shows by how much the outcome (i.e CCI, CIre, NDII or NIRV) on the *asinh* scale changes within a plot and year, for a one-unit increase in the driver on the *asinh* scale, at the environmental conditions of the focal pixel. Including the same within-demeaned controls as described above ensured numerical comparability of average effects. The spatial variation around that average was then attributed to the static environment via the varying-coefficient terms.

S4 - Comparing with LMM and TWFE approach for modelization

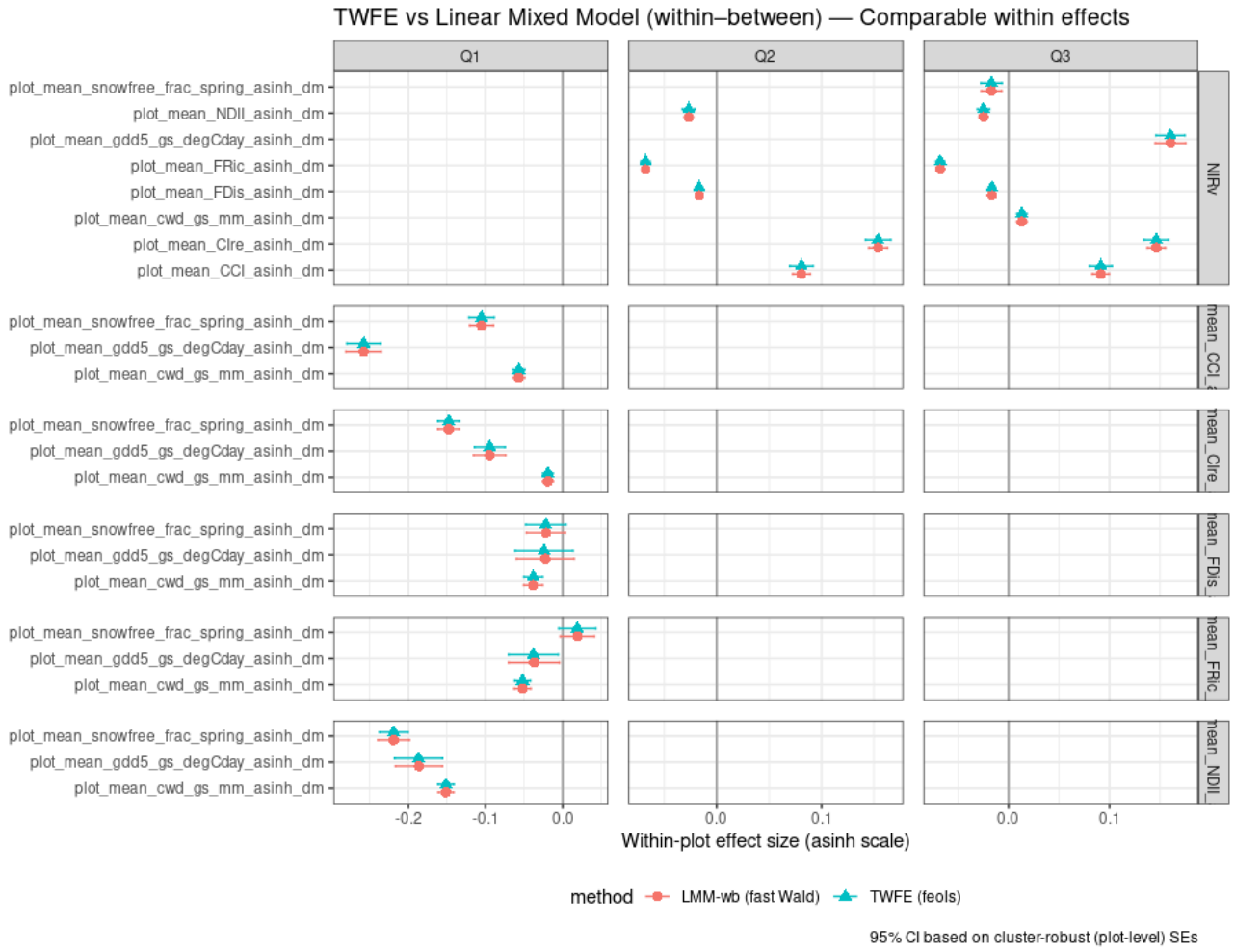

Across all links (Q1 climate → traits, Q2 traits → NIRv, Q3 climate → NIRv conditional on traits), the two-way fixed-effects (TWFE) estimates (teal triangles) and the demeaned LMM estimates (salmon circles) are virtually indistinguishable in both magnitude and sign, with overlapping 95% cluster-robust CIs throughout . No coefficient changes sign, and any differences are below the plotting resolution. This equivalence is expected because model specifications target the same within-plot parameter. TWFE with plot and year fixed effects is algebraically the within (demeaned) estimator: it removes all between-plot and common-year variation and fits OLS to the plot-demeaned regressors and outcomes. The LMM used in the main analyses is parameterized in a within–between decomposition and we report the within (demeaned) slope; with only a random intercept (no random slopes) and cluster-robust (plot-level) standard errors, the GLS/LMM coefficient on the within component coincides with the TWFE coefficient under standard regularity conditions (strict exogeneity after FE, many plots, no small-T bias in levels). Because both models use the same set of controls (year effects, same covariates) and inference is based on plot-clustered SEs, the resulting point estimates and uncertainty are effectively the same. Minor numerical differences can arise from weighting/df conventions (REML vs. OLS, Satterthwaite vs. HC/CRV variance), but they are immaterial here. For our panel of Alpine grasslands, conclusions about climate–biodiversity–productivity links do not depend on whether we use TWFE or a demeaned LMM: both recover the same short-term, within-plot sensitivities while controlling for unobserved, time-invariant plot characteristics and common year shocks.

S5 - Decomposition of climate effects into direct, indirect, and total components

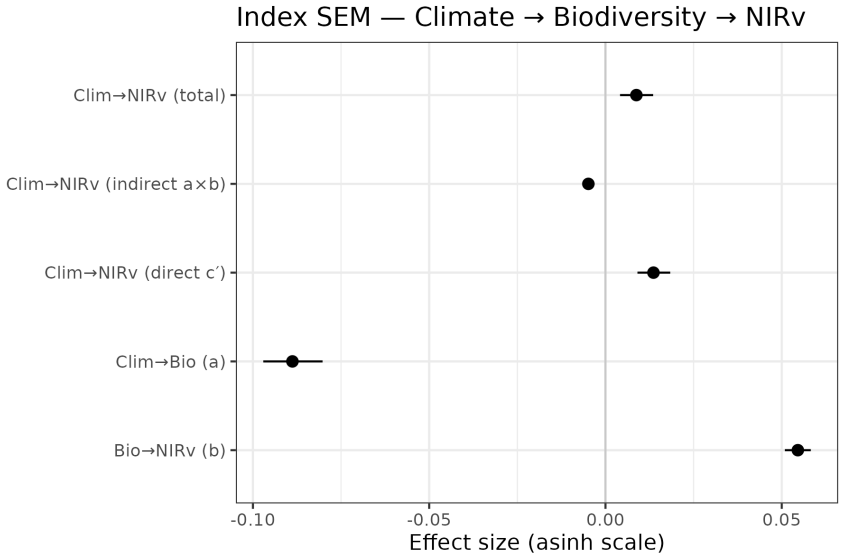

Standardized effect sizes (asinh scale) from the structural equation model showing the total effect of climatic drivers on NIRv (Clim → NIRv, total), its direct component (Clim → NIRv, direct c'), and its indirect component mediated by canopy functional structure (Clim → Bio → NIRv, indirect a×b). Indirect effects correspond to the product of the climate → biodiversity and biodiversity → productivity paths. Points represent estimated effects and horizontal bars indicate 95% confidence intervals.

S6 - Indirect climate effects, decomposed by mediator

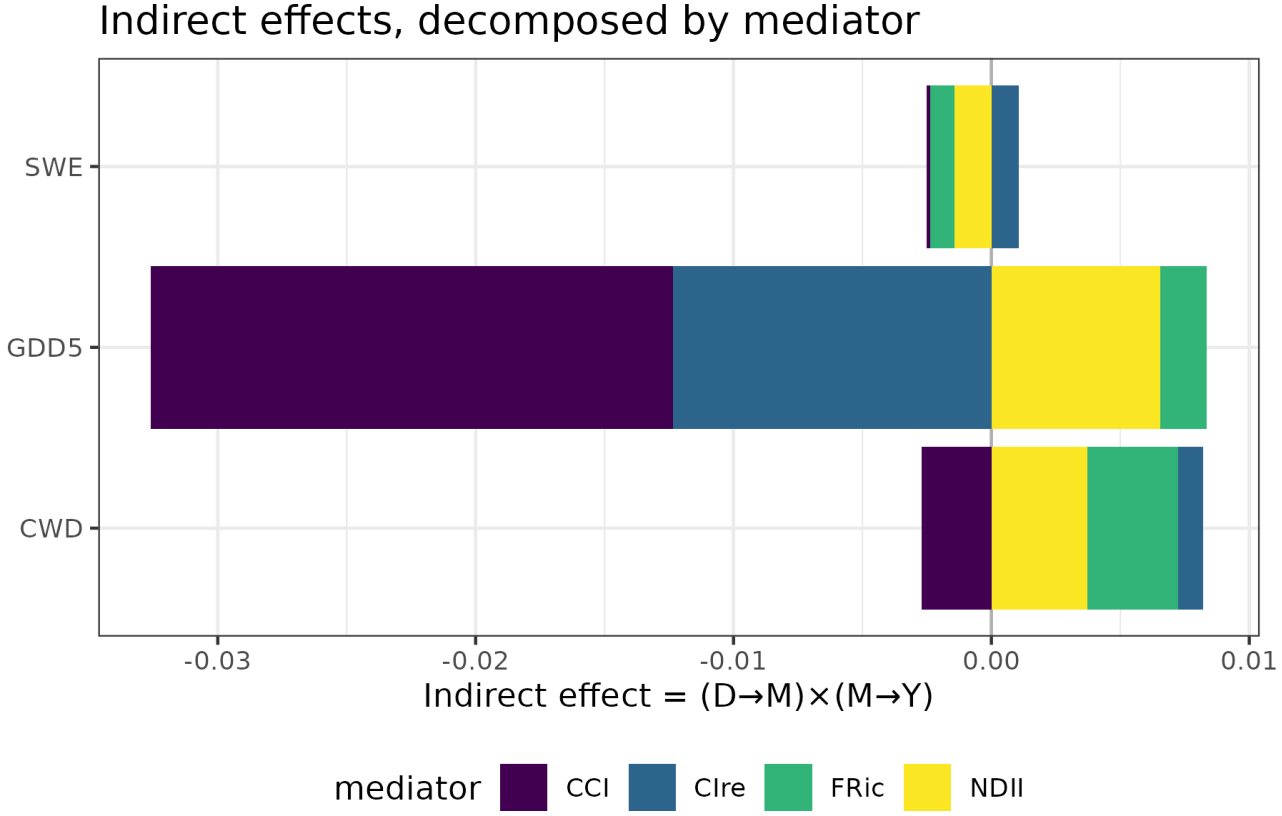

Indirect effects of interannual climate anomalies on NIRv, decomposed by canopy functional mediators. For each climatic driver (GDD, CWD, SWE), indirect effects are shown as the product of the climate → mediator path and the mediator → NIRv path (a×b), and are partitioned among chlorophyll-related spectral composition (CIre), photoprotective pigment investment (CCI), canopy water status (NDII), and spectral functional richness (FRic). Bar lengths indicate standardized indirect effect sizes (asinh scale), with positive and negative contributions shown by direction along the x-axis.

S7 - Environmental controls and mapping

GDD → NDII

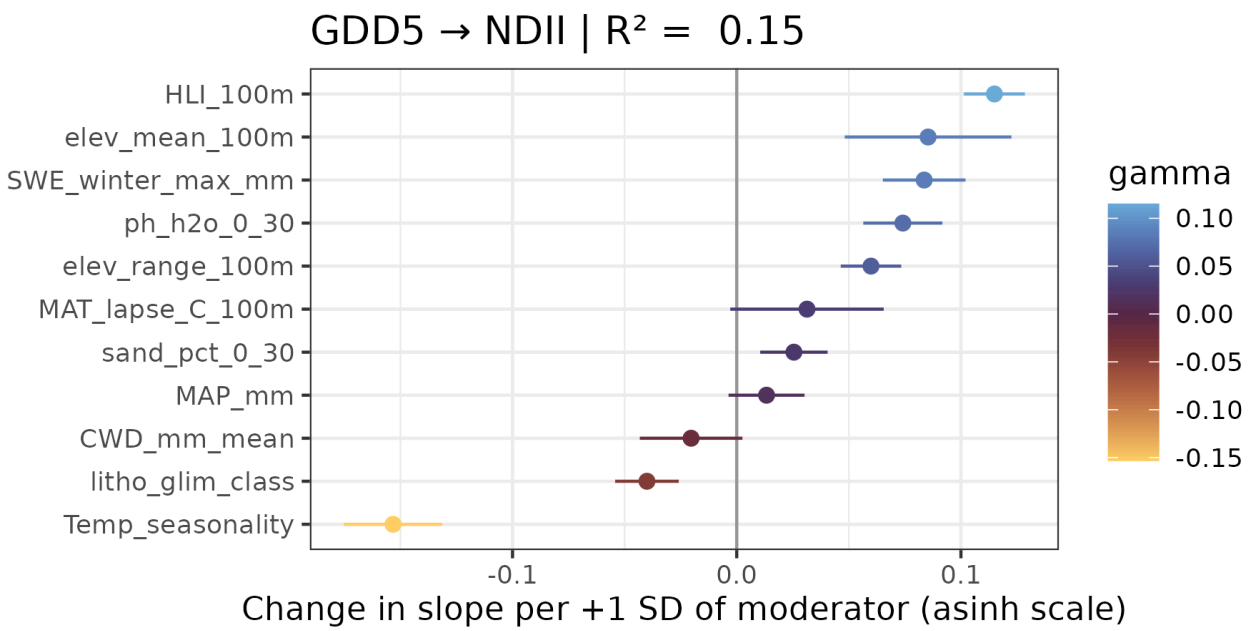

Environmental moderators of the within-plot slope GDD→NDII estimated from the varying-effect LMM. Points are environmental effect coefficients, i.e change in GDD

→NDII effect per +1 SD of the moderator (with 95% CIs).

Results description: On average, warmer growing seasons reduce NDII within plots, but this sensitivity varies with the environment which explains 15% of the plot-to-plot variation in the GDD⟶NDII effect. Temperature seasonality amplified GDD → NDII negative effects : in continental sectors, warm years push NDII down the most. Topographic (HLI, mean elevation, elevation range) and soil (soil pH). Note that apart from temperature seasonality, climatic variables such as MAT, CWD and MAP had very little to null effect.

Ecological interpretation: NDII proxies leaf water content. Strong negative GDD⟶NDII where seasonality is high fits expected VPD/phenology mechanism: warmer years bring higher atmospheric demand and earlier exposure to midsummer dryness. Snowpack, topographic heterogeneity, elevation, and insolation reduce the marginal drying per added heat, yielding weaker or neutral slopes.

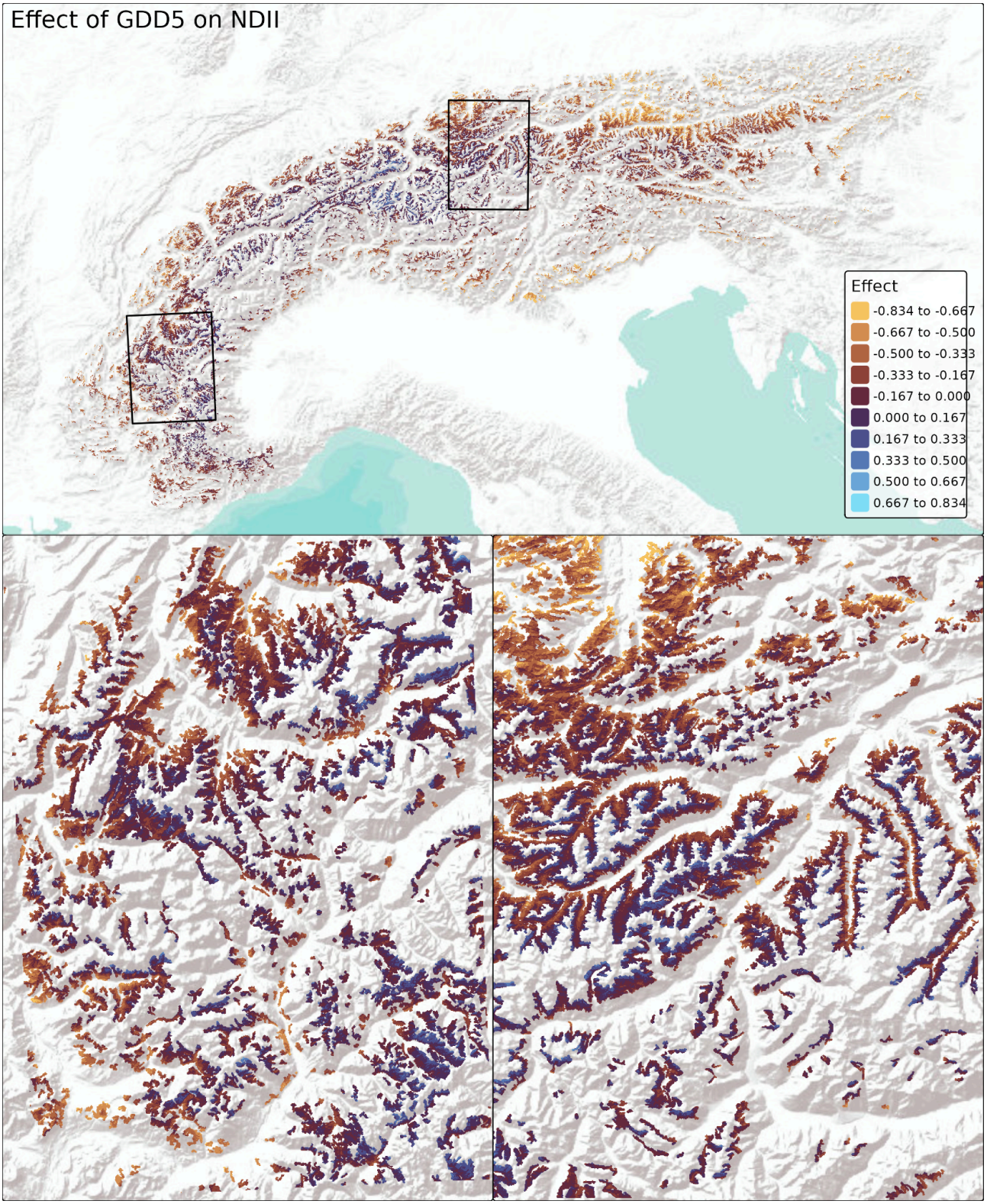

Predicted spatial distribution of the within-plot GDD→NDII effect from the varying-coefficient LMM. Colors show the magnitude and sign of the GDD→NDII slope on the asinh scale (blue = more negative; orange = more positive).

When transferred to geographic space, environmental control on the GDD ⟶ NDII effect revealed more negative effects in north–eastern and external areas (orange). This matches the negative moderation by temperature seasonality : in more continental areas, a warm year translates into a sharper drop in canopy water content. By contrast, in south-western arc and inner areas the negative effect was weak to null (purple), consistent with moderators that buffer dehydration (at 100m resolution) : high elevation, greater winter SWE, stronger local relief. The bottom panels reveal the fine-scale imprint of topography. In the right

(central–eastern) inset, valley bottoms appear more orange (more negative slopes) while crests and high passes are purple then blue, echoing elevation's positive γ (higher elevation attenuates the NDII decline). In both insets, south-facing slopes (high HLI) tend to show more blue (i.e weaker response) whereas north-facing slopes remain more orange (more negative), in line with HLI's strong positive moderation. Snow-influenced divides and plateaus show localized buffering (bluish rims) consistent with the positive γ for SWE. Substrate signals are subtler: more alkaline/calcareous bands (higher pH; γ > 0) read slightly cooler than adjacent siliceous belts, while lithology itself adds a small extra sharpening (γ = −0.0368 [−0.0508, −0.0227]), so lithologic mosaics appear as faint orange streaks rather than dominant features. In our SEM, NDII increase affects negatively NIRv; hence regions with bluer maps contribute a larger positive NDII-mediated piece to warming's net effect on productivity, while warmer patches contribute little through this pathway.

CIre→NIRv

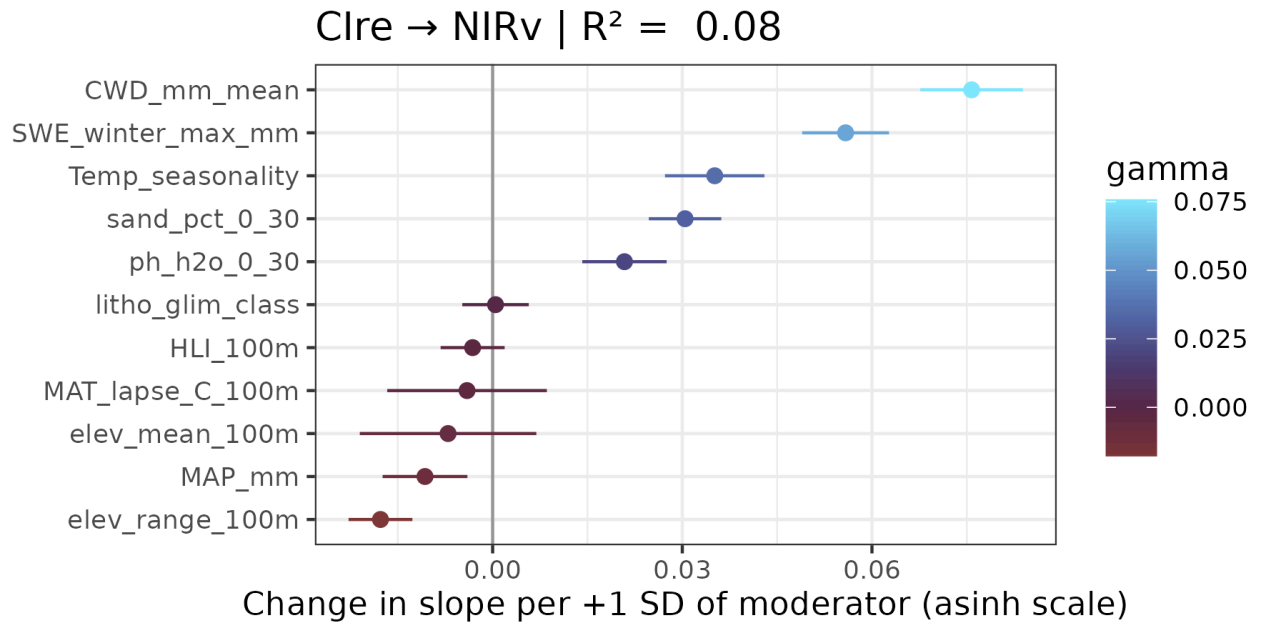

Static moderators of the within-plot effect of **CIre on NIRv** from the varying-coefficient LMM. Points are γ estimates (change in the CIre→NIRv slope per +1 SD of each standardized moderator) with 95% CIs. Positive γ means the CIre→NIRv coupling becomes **stronger (more positive)** as the moderator increases; negative γ means it becomes **weaker**.

Results description: across plots and years the CIre → NIRv slope is positive, and its strength varies weakly with the static environment which only explains 8% of the plot-to-plot variation. Several moderators reinforce this coupling (positive γ): baseline aridity, CWD (γ = +0.0758, 95% CI [0.0676, 0.0839]), winter SWE (+0.0558 [0.0489, 0.0627]), temperature seasonality (+0.0351 [0.0273, 0.0430]), sand fraction (+0.0304 [0.0247, 0.0362]), and soil pH (+0.0208 [0.0142, 0.0275]). Two moderators weaken the link (negative γ): terrain ruggedness (elev_range_100m) (γ = −0.0177 [−0.0228, −0.0127]) and MAP (−0.0107 [−0.0174, −0.0040]).

Ecological interpretation: CIre tracks chlorophyll-related photosynthetic capacity. Where water limitation and short effective seasons dominate (higher CWD, SWE and seasonality), small interannual increases in canopy chlorophyll translate into large gains in NIRv, hence the positive γ's. Coarser and more alkaline soils (sand, pH) likely accentuate nutrient–water constraints, so canopy photosynthetic capacity becomes a tighter rate-limiter of realized productivity. In contrast, in wetter backgrounds (high MAP) or rugged terrain that mixes aspects, soils and phenologies at fine scales, the canopy-scale CIre signal is diluted when integrated to productivity, weakening the CIre–NIRv coupling.

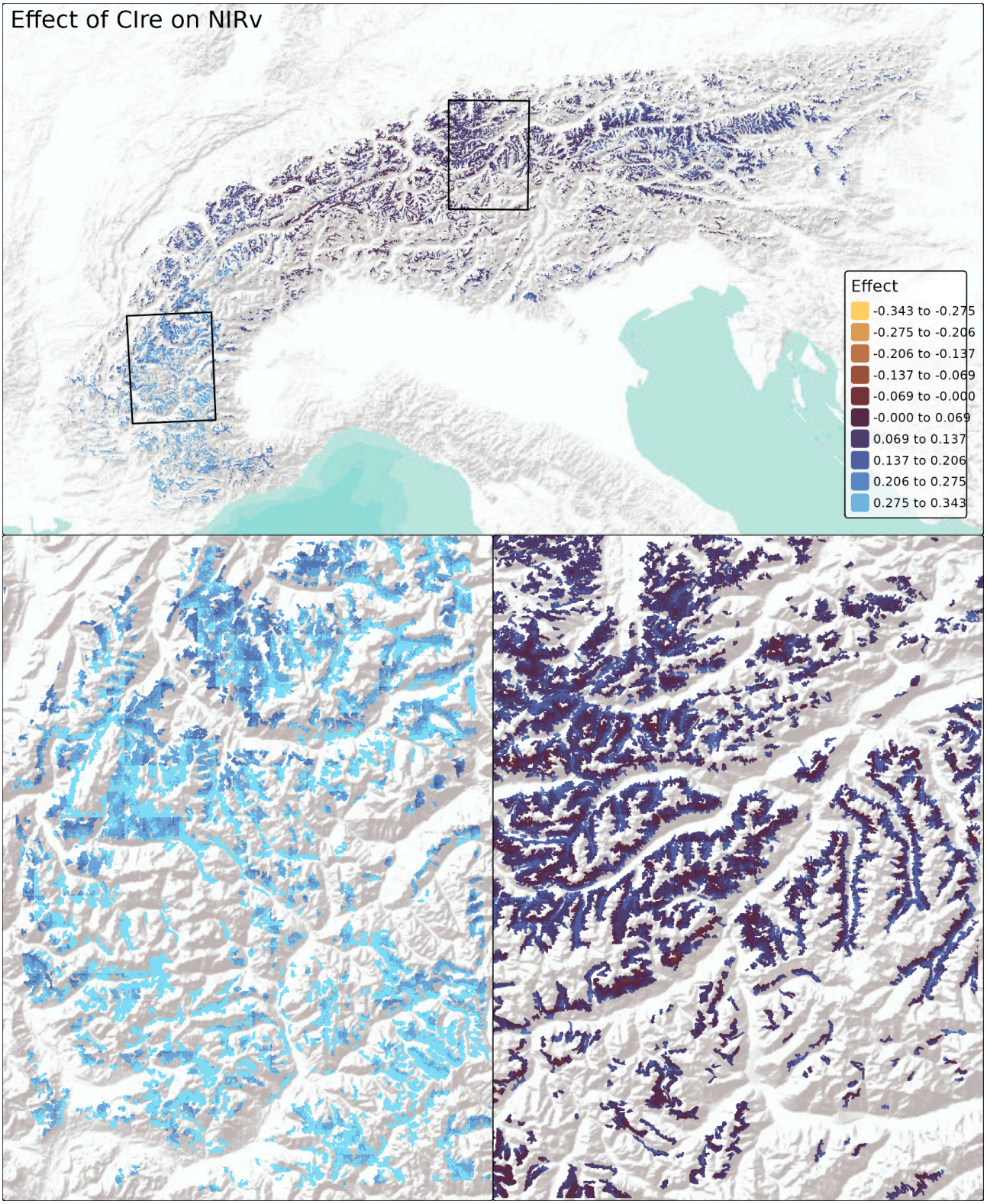

Transfer to geographic space: The map is dominated by purple and dark blue, with very little orange/yellow. This indicates a widespread positive CIre → NIRv coupling and only modest macro-scale heterogeneity. Where light blue hotspots appear (south-western Alps and in eastern interior ranges) they coincide with combinations of moderators that strengthen the link in the coefficient table: higher CWD, more SWE, or stronger temperature seasonality , and soil contexts with higher sand and pH. Conversely, belts that revert toward purple (weaker coupling) align with conditions that weaken the slope : wetter corridors (MAP) and rugged terrain (elev_range).

The insets show that meso- to local-scale structure is present but not dominant. In both zooms, coherent light-blue tracts follow snow-influenced divides or drier interior basins, consistent with positive γ for SWE, seasonality, and CWD. Areas with high relief tend to shift back toward purple, matching the negative γ for terrain ruggedness : micro-topographic mixing blunts how canopy chlorophyll gains translate into productivity. Systematic aspect or altitudinal bands are weak to absent, which fits the non-significant γ for HLI and mean elevation; likewise, MAT_lapse and lithology leave little visible imprint (γ ≈ 0). Overall, the map conveys a domain-wide positive CIre → NIRv relationship with patchy strengthening where seasonality/snow/aridity and coarse, alkaline substrates co-occur, and dampening in wetter, highly rugged belts, as implied by the moderation coefficients.

FRic→NIRv

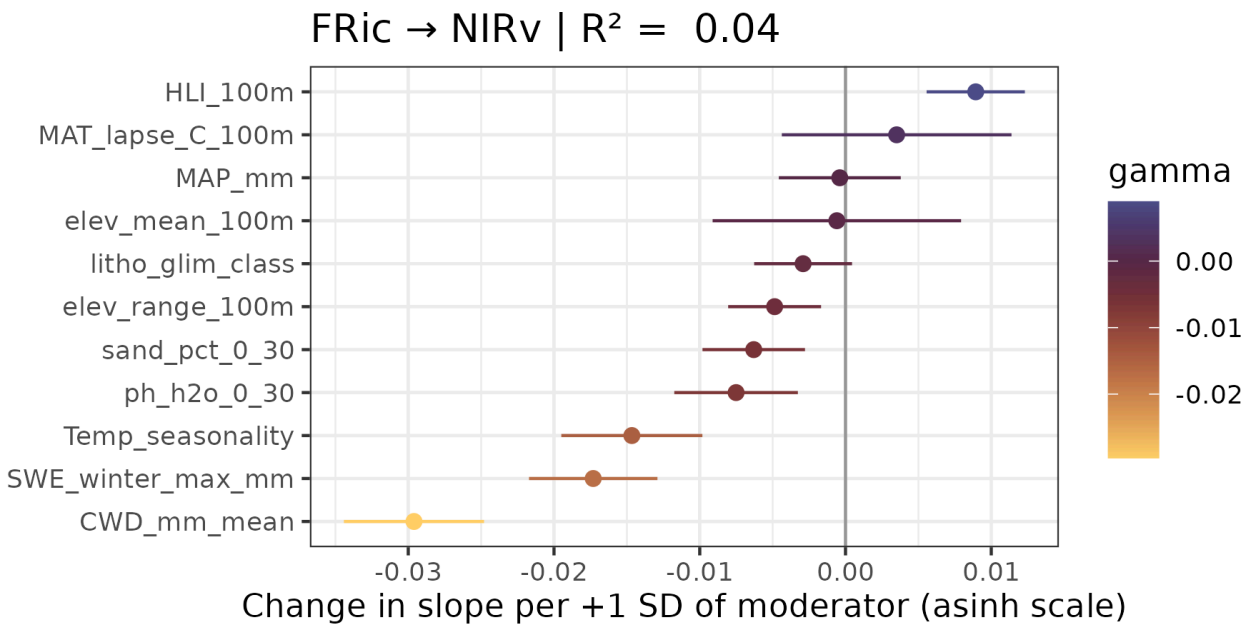

Coefficient plot. Static moderators of the **FRic→NIRv** slope. Positive γ strengthens (moves toward zero or positive) the FRic–productivity coupling; negative γ makes it

Results description: across plots and years the FRic → NIRv slope is negative on average, with static environment explaining only 4% of the plot-to-plot variation on effects.Most environmental moderators make the FRic → NIRv more negative. The strongest sharpeners are baseline aridity (CWD), winter snow water equivalent (SWE), and temperature seasonality. Additional (smaller) negative moderations come from soil pH, sand fraction, and local terrain ruggedness (elev_range_100m). One moderator attenuates the negativity: solar exposure (HLI).

Ecological interpretation: at interannual scales, increases in functional richness (FRic) likely reflect turnover and phenological mixing rather than immediate boosts to canopy photosynthetic capacity. Under strong climatic constraints (high CWD, high SWE), years with higher FRic tend to coincide with lower NIRv, plausibly because communities shift toward stress-tolerant strategies and/or become more asynchronous in phenology, reducing the integrated NIRv signal. Coarse or alkaline soils and rugged micro-topography accentuate this decoupling, while high insolation (HLI) slightly mitigates it, perhaps because radiation alleviates light limitation so that differences in species traits translate less into a penalty for whole-canopy productivity. In the broader causal framing, this confirms that the FRic b-path is generally weak and negative, much less influential than pigment-based proxies (CIre/CCI) for explaining year-to-year productivity.

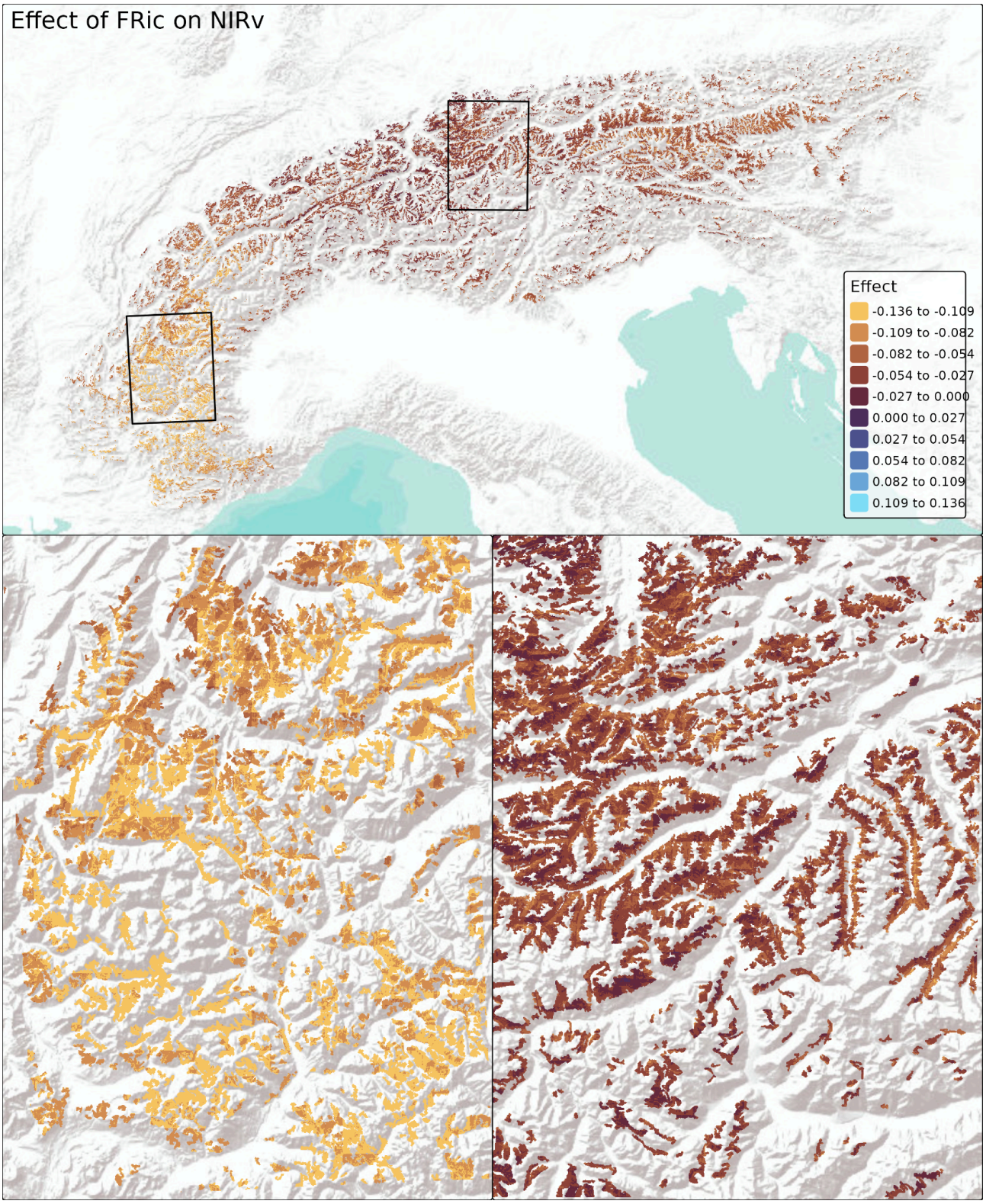

Transfer to geographic space: the map is dominated by yellow–orange, with almost no blue, confirming a domain-wide negative FRic→NIRv coupling and only modest macro-scale heterogeneity. Where the map shifts toward lighter yellow (most clearly in the south-western inset) the penalty is stronger (more negative). That spatial concentration matches the moderators with negative γ that sharpen the slope: higher CWD, more alkaline/coarser soils (pH and sand effects)), and greater ruggedness (elev_range). In these SW basins and dissected slopes, years with higher FRic align with lower NIRv, pushing colors to light

yellow. By contrast, the central–eastern inset is darker orange to purple, indicating a weaker (less negative) or near-zero coupling. This is consistent with lower aridity locally (smaller influence of CWD, the strongest negative moderator) and with higher insolation on ridges where the only positive moderator (HLI) attenuates the penalty. Within this region, the expected sharpeners (SWE; temperature seasonality) do appear as lighter streaks on some snow-prone crests, but the net effect across the inset remains darker than in the SW, implying that aridity/soil controls dominate the geography of the FRic penalty. At local scales, patterns are present but light: sun-exposed benches and crests tend to be darker (less negative) than adjacent shaded flanks (HLI > 0), while rough, dissected terrain shifts lighter than smoother neighbors (negative effect for elev_range). Bands of calcareous substrate (higher pH) read lighter than nearby siliceous belts, consistent with the small but significant negative γ. Moderation by MAP, mean elevation, lithology and MAT_lapse is weak (effect ≈ 0), which explains why large-scale precipitation or simple altitudinal gradients leave only faint cartographic imprints.